PERGAMON

International Journal of Solids and Structures 39 (2002) 499–528

INTERNATIONAL JOURNAL OF SOLIDS and STRUCTURES

www.elsevier.com/locate/ijsolstr

Covariant principal axis formulation of associated coupled thermoplasticity at finite strains and its numerical implementation

Adnan Ibrahimbegovic [a,*], Lotfi Chorfi [b]

[a] *Ecole Normale Supérieure de Cachan, LMT, 61 av. du président Wilson, 94235 Cachan Cedex, France*
[b] *Dépt. GSM, Université de Technologie de Compiègne, bp-529, 60205 Compiègne, France*

Received 6 July 2000

Abstract

In this work we discuss a covariant formulation of the finite strain viscoplasticity in a fully coupled thermomechanical setting. The formulation is presented within the framework of the principal axis methodology, which leads to a very efficient numerical implementation. Several numerical simulations, dealing with fully coupled thermomechanical response at large viscoplastic strains and including both strain localization and cyclic loading cases, are presented in order to illustrate a very satisfying performance of the proposed methodology. © 2001 Published by Elsevier Science Ltd.

Keywords: Thermomechanical coupling; Plasticity; Finite deformation

1. Introduction

In this paper we carry on with the development of finite deformation plasticity theory on a manifold, much in the spirit of our recent works (e.g. see Ibrahimbegovic (1994) and Ibrahimbegovic and Gharzeddine (1998)) which show how the principal axis methodology of Hill (1978) can be applied to manifolds to simplify the tensor analysis to a bit more than a manipulation of scalars. Our main goal in this work is to develop a covariant formulation of the coupled thermoplasticity at finite strains, i.e. to take into account the practical situations where finite deforming elastoplastic solids is also exposed to a variation of a temperature field, or where some of the plastic work would transfer into heating.

The salient features of the finite deformation plasticity model discussed herein are as follows: (i) the multiplicative decomposition (see Lee (1969) or Mandel (1973)), which allows for finite elastic and finite plastic deformation; (ii) isotropy of the elastic response, which is a reasonable hypothesis (e.g. see Drucker

* Corresponding author. Tel.: +33-1-4740-2234; fax: +33-1-4740-2240.
E-mail address: ai@lmt.ens-cachan.fr (A. Ibrahimbegovic).

0020-7683/01/$ - see front matter © 2001 Published by Elsevier Science Ltd.
PII: S0020-7683(01)00221-9

(1988)) for a vast majority of metals and alloys; (iii) generalization of the principle of the maximum plastic dissipation (e.g. see Hill (1950) or Lubliner (1984)) to the thermomechanical setting.

A number of recent works dealing with the thermoplasticity formulation at finite strains share similar features with this model, starting with the pioneering work of Argyris et al. (1982), where multiplicative decomposition of the deformation gradient is assumed but not exploited in computations. Some representative works in that respect are those of Lubliner (1984), Iman and Johnson (1998) and Wriggers et al. (1992) proposing the appropriate forms of the deformation gradient for finite deformation thermoplasticity, or Simo and Miehe (1992) and Armero and Simo (1993) who also address the numerical implementation. The model of finite strain thermoplasticity discussed herein is developed along the same lines.

The main novelty with respect to those works on the side of theoretical formulation concerns the chosen manifold setting and the principal axis methodology. Such a formulation provides a very suitable framework for the subsequent numerical solution of the problem in that one can uncouple the geometric from material nonlinearities and thus simplify the plastic flow computation, as already demonstrated by a number of recent works in a somewhat simpler, purely mechanical setting (e.g. see Weber and Anand (1990), Eterovic and Bathe (1990), Cuitino and Ortiz (1992), Perić et al. (1992), Simo (1992), Miehe and Stein (1992) or Ibrahimbegovic (1994) and Ibrahimbegovic and Gharzeddine (1998), among others).

An additional novel aspect of the proposed formulation concerns the role of the elastic entropy variable, which is given through its 'constitutive equation', and which is thus employed in a very similar manner as the stress tensor providing a better structure the governing equations.

The outline of the paper is as follows. In Section 2 we develop all the governing equations of the proposed model of coupled thermoplasticity at finite strain. In Sections 2.5 and 2.6 we present the consistent linearization of the governing equations, which form the basis of any Newton like iterative solution scheme. A model problem for the finite element discretization corresponding to an axisymmetric finite element is presented in Section 2.4. Section 3 gives several illustrative numerical examples. Some concluding remarks are stated in Section 4.

2. Formulation of coupled thermoplasticity on a manifold

2.1. Basic hypotheses

In this section we develop the governing equations for the proposed, fully coupled thermoplasticity model at finite strain. The finite deformation kinematics, which allows for any size of the elastic and plastic deformations relies on the multiplicative decomposition of deformation gradient (e.g. see Lee (1969) and Mandel (1973)).

$$\boldsymbol{F} = \boldsymbol{F}^{\mathrm{e}}\boldsymbol{F}^{\mathrm{p}} \tag{1}$$

where $\boldsymbol{F}^{\mathrm{e}}$ and $\boldsymbol{F}^{\mathrm{p}}$ are elastic and plastic part. Such a decomposition gives rise to so-called intermediate stress-free configuration, which is supposed to be recovered upon eventual elastic unloading (carried out by $\boldsymbol{F}^{\mathrm{e}}$).

In the proposed plasticity model we assume that the amount of plastic flow does not affect the elastic response, but that stress change does influence the elastic domain (where $\boldsymbol{F}^{\mathrm{p}}$ would not change) through hardening phenomena (e.g. see Hill (1950)). For simplicity, we consider only isotropic hardening with a uniform increase of elastic domain without changing its shape, which can be represented by a scalar internal variable to be denoted as ξ. For the appropriate manner to incorporate the kinematic hardening phenomena, in the present theory of finite deformation plasticity, we refer to our recent work (see Ibrahimbegovic and Chorfi (2000)).

Finally, in order to account for temperature change and thermomechanical coupling we need to introduce an additional state variable in terms of entropy (e.g. see Truesdell and Noll (1965) or Ericksen (1998)), which we denote as η. However, since it is generally accepted in thermodynamics that entropy is additive or so-called extensive variable (see Ericksen (1998, p. 11)), we postulate that the total entropy could be decomposed to the elastic and plastic part

$$\eta = \eta^{\mathrm{e}} + \eta^{\mathrm{p}} \tag{2}$$

One should note that the role of entropy is quite a controversial issue in thermodynamics, except when we deal with reversible processes. Our assumption in Eq. (2) above pertains to irreversible processes and is possibly the simplest form that follows in the footsteps of Simo and Miehe (1992) and Armero and Simo (1993), assuming that the plastic entropy η^{p} is an internal variable which accounts for the change of flow criterion with respect to temperature and related dissipative plastic structural changes.

In conclusion, for a finite strain thermoplasticity model of this kind we can define the internal energy, $e(\cdot)$, as a function of the listed state variables, $\boldsymbol{F}^{\mathrm{e}}$, ξ and η^{e}, according to

$$e(\boldsymbol{F}^{\mathrm{e}}, \mathbf{g}, \xi, \eta^{\mathrm{e}}) \tag{3}$$

where the metric tensor, $\mathbf{g}$, should also be included in the list, when we work in manifolds in order to allow for a set of general nonlinear coordinates.

By following Drucker (1988), we assume that the elastic response is isotropic, which implies that the internal energy governing the stress computation should remain invariant under a rigid body motion superposed on the intermediate configuration, resulting with the appropriate transformation of $\boldsymbol{F}^{\mathrm{e}} \to \boldsymbol{F}^{\mathrm{e}^+} = \boldsymbol{F}^{\mathrm{e}}\mathbf{Q}$, where $\mathbf{Q}$ is the corresponding orthogonal tensor ($\mathbf{Q}^{\mathrm{T}} = \mathbf{Q}^{-1}$). In order to meet such an invariance requirement, the internal energy should be reduced to a function of the left Cauchy–Green elastic deformation tensor, $\mathbf{b}^{\mathrm{e}} = \boldsymbol{F}^{\mathrm{e}}\bar{\mathbf{G}}^{-1}\boldsymbol{F}^{\mathrm{e}^{\mathrm{T}}}$ with $\mathbf{b}^{\mathrm{e}^+} = \mathbf{b}^{\mathrm{e}}$, so that we can write

$$e(\mathbf{b}^{\mathrm{e}}, \mathbf{g}, \xi, \eta^{\mathrm{e}}) \tag{4}$$

Further restriction on the form of internal energy is placed by the standard objectivity requirements, or the invariance requirements under the rigid body motion superposed on the current configuration (e.g. see Gurtin (1981, p. 143)), which results with

$$e(\lambda_i^{\mathrm{e}}, \xi, \eta^{\mathrm{e}}) \tag{5}$$

where λ_i^{e}, $i = 1, 2, 3$ are the elastic principal stretches. The latter is selected as a possible invariant representation of the tensor pair, $\mathbf{b}^{\mathrm{e}}$ and $\mathbf{g}$, which can be computed as the solution of the eigenvalue problem

$$[\mathbf{b}^{\mathrm{e}} - (\lambda_i^{\mathrm{e}})^2\mathbf{g}^{-1}]\boldsymbol{v}_i = \mathbf{0} \tag{6}$$

where $\boldsymbol{v}_i$ are the corresponding principal covectors or one-forms (see Ibrahimbegovic (1994)). The latter share the generalized orthogonality property

$$\boldsymbol{v}_i \cdot \mathbf{g}^{-1}\boldsymbol{v}_j = \delta_{ij} := \begin{cases} 1, & i = j \\ 0, & i \neq j \end{cases} \tag{7}$$

which allows us to construct the spectral decomposition of $\mathbf{b}^{\mathrm{e}}$ as

$$\mathbf{b}^{\mathrm{e}} = \sum_{i=1}^{3} (\lambda_i^{\mathrm{e}})^2 \mathbf{g}^{-1}\boldsymbol{v}_i \otimes \mathbf{g}^{-1}\boldsymbol{v}_i \tag{8}$$

We note in passing that the isotropy of the elastic response further implies that the corresponding thermodynamically conjugate stress tensor is the Kirchhoff stress $\boldsymbol{\tau} = J\boldsymbol{\sigma}$, where $\boldsymbol{\sigma}$ is the Cauchy or true stress and $J = \det \boldsymbol{F}$, and that the Kirchhoff stress tensor shares the same eigenvectors, i.e.

$$[\boldsymbol{\tau} - \tau_i \mathbf{g}^{-1}]\boldsymbol{v}_i = \mathbf{0} \;\Rightarrow\; \boldsymbol{\tau} = \sum_{i=1}^{3} \tau_i \mathbf{g}^{-1}\boldsymbol{v}_i \otimes \mathbf{g}^{-1}\boldsymbol{v}_i \tag{9}$$

where τ_i are the principal values of Kirchhoff stress.

We also follow the often invoked modification to replace the entropy from the list of state variables by the absolute temperature θ. The latter can be achieved by appealing to the Legendre transformation, and abandoning the internal energy in favor of the free energy $\psi(\cdot)$ according to

$$\psi(\lambda_i^{\mathrm{e}}, \xi, \theta) = e(\lambda_i^{\mathrm{e}}, \xi, \eta^{\mathrm{e}}) - \theta\eta^{\mathrm{e}} \tag{10}$$

We note in passing that the assumption on the elastic response which is not affected by the amount of plastic deformation leads to an uncoupled form of the free energy

$$\psi(\lambda_i^{\mathrm{e}}, \xi, \theta) = \tilde{\psi}(\lambda_i^{\mathrm{e}}, \theta) + \chi(\xi, \theta) \tag{11}$$

where the second term in Eq. (11) accounts for temperature dependent hardening effects. However, this kind of decomposition is not essential for the subsequent considerations.

To complete the description of the proposed general form of the coupled thermoplasticity model we need to define the elastic domain, where no change in plastic deformation or hardening variable would take place. The latter corresponds to negative values of the yield function $\phi(\cdot)$

$$\phi(\boldsymbol{\tau}, \mathbf{g}, q, \theta) < 0 \tag{12}$$

where q is flux thermodynamically conjugate to the hardening variable ξ. Due to isotropy of the elastic response, we can recover not only the result in Eq. (9), but also an invariant form of the yield criterion, which can also be expressed in terms of the principal values of the Kirchhoff stress

$$\phi(\tau_i, q, \theta) < 0 \tag{13}$$

2.2. Reduced dissipation inequality and the principle of maximum plastic dissipation

In summary of the foregoing considerations we can conclude that the primary or state variables are the absolute temperature θ, hardening variable ξ, the left Cauchy–Green elastic deformation tensor $\mathbf{b}^{\mathrm{e}}$ and metric tensor $\mathbf{g}$, with the last two jointly represented by the elastic principal stretches λ_i^{e}.

The dependent variables to be obtained from the state variables are: the Kirchhoff stress tensor $\boldsymbol{\tau}$ (represented by its principal values), the hardening flux q and the elastic and plastic entropy η^{e} and η^{p}.

This dependence on state variables is not arbitrary and has to be constructed in accordance with the second law of thermodynamics, which can be stated in the form of Clausius–Duhem inequality (e.g. see Marsden and Hughes (1983, p. 176)) as

$$\theta\gamma := \theta\dot{\eta} + \boldsymbol{\tau}\cdot\mathbf{d} - \dot{e} - \mathbf{q}\cdot\nabla^{\varphi}\theta/\theta \geqslant 0 \tag{14}$$

In Eq. (14) above, $\mathbf{d}$ is the rate-of-deformation tensor, which can be computed as the Lie derivative of the metric tensor (e.g. see Marsden and Hughes (1983, p. 109)) as

$$\begin{aligned} \mathbf{d} &= \tfrac{1}{2}L_v[\mathbf{g}] := \tfrac{1}{2}\boldsymbol{F}^{-\mathrm{T}}\frac{\partial}{\partial t}(\boldsymbol{F}^{\mathrm{T}}\mathbf{g}\boldsymbol{F})\boldsymbol{F}^{-1} \\ &= \tfrac{1}{2}(\dot{\mathbf{g}} + \mathbf{g}\mathbf{l} + \mathbf{l}^{\mathrm{T}}\mathbf{g}) \end{aligned} \tag{15}$$

where $\mathbf{l} = \dot{\boldsymbol{F}}\boldsymbol{F}^{-1}$ is the spatial velocity gradient. Moreover, $\mathbf{q}$ in Eq. (14) above denotes the Kirchhoff-like heat flux (the spatial heat flux times the Jacobian of the deformation). It is assumed that the heat flux is given by the generalized Fourier law and that the absolute temperature is always positive, so that the last term in Eq. (14) above is always nonnegative

$$\theta > 0 \text{ and } \mathbf{q} = -k\nabla^{\varphi}\theta, \ k > 0 \ \Rightarrow \ \mathbf{q}\cdot\nabla^{\varphi}\theta/\theta \geqslant 0 \tag{16}$$

which allows us to obtain the Clausius–Plank form (e.g. see Truesdell and Noll (1965, p. 159)) of the second law, defining the total dissipation as

$$\mathscr{D} := \theta\dot{\eta} + \boldsymbol{\tau}\cdot\mathbf{d} - \dot{e} \geqslant 0 \tag{17}$$

By appealing the Legendre transformation in Eq. (10) and making use of the additive split of the total entropy in Eq. (2), we can rewrite the total dissipation in the following form

$$\mathscr{D} := \theta\dot{\eta}^{\mathrm{p}} - \dot{\theta}\eta^{\mathrm{e}} + \boldsymbol{\tau}\cdot\mathbf{d} - \dot{\psi} \geqslant 0 \tag{18}$$

The last term in Eq. (18) above denotes the material time derivative of the free energy, which can be computed by the chain rule with respect to the given set of state variables

$$\dot{\psi} = 2\frac{\partial\psi}{\partial\mathbf{g}}\cdot\mathbf{d} + \frac{\partial\psi}{\partial\mathbf{b}^{\mathrm{e}}}\cdot L_v[\mathbf{b}^{\mathrm{e}}] + \frac{\partial\psi}{\partial\xi}\dot{\xi} + \frac{\partial\psi}{\partial\theta}\dot{\theta} \tag{19}$$

where $\mathbf{d}$ is defined by Eq. (15), whereas the Lie derivative of $\mathbf{b}^{\mathrm{e}}$ can be computed as

$$L_v[\mathbf{b}^{\mathrm{e}}] := \boldsymbol{F}\frac{\partial}{\partial t}[\boldsymbol{F}^{-1}\mathbf{b}^{\mathrm{e}}\boldsymbol{F}^{-\mathrm{T}}]\boldsymbol{F}^{\mathrm{T}} = \dot{\mathbf{b}}^{\mathrm{e}} - \mathbf{l}\mathbf{b}^{\mathrm{e}} - \mathbf{b}^{\mathrm{e}}\mathbf{l}^{\mathrm{T}} \tag{20}$$

With this result on hand the total dissipation can be recast as

$$\mathscr{D} := \left(\boldsymbol{\tau} - 2\frac{\partial\psi}{\partial\mathbf{g}}\right)\cdot\mathbf{d} + \left(-\eta^{\mathrm{e}} - \frac{\partial\psi}{\partial\theta}\right)\dot{\theta} - \frac{\partial\psi}{\partial\mathbf{b}^{\mathrm{e}}}\cdot L_v[\mathbf{b}^{\mathrm{e}}] - \frac{\partial\psi}{\partial\xi}\dot{\xi} + \theta\dot{\eta}^{\mathrm{p}} \geqslant 0 \tag{21}$$

For all the states which remain within elastic domain, defined with $\phi(\cdot) < 0$, the values of plastic deformation (and associated intermediate configuration) would not change. By means of Eqs. (1) and (4) we thus obtain

$$L_v[\mathbf{b}^{\mathrm{e}}] = \boldsymbol{F}\frac{\partial}{\partial t}[\underbrace{\boldsymbol{F}^{\mathrm{p}^{-1}}\boldsymbol{F}^{\mathrm{e}^{-1}}}_{\boldsymbol{F}^{-1}}\underbrace{\boldsymbol{F}^{\mathrm{e}}\bar{\mathbf{G}}^{-1}\boldsymbol{F}^{\mathrm{e}^{\mathrm{T}}}}_{\mathbf{b}^{\mathrm{e}}}\underbrace{\boldsymbol{F}^{\mathrm{e}^{-\mathrm{T}}}\boldsymbol{F}^{\mathrm{p}^{-\mathrm{T}}}}_{\boldsymbol{F}^{-\mathrm{T}}}\boldsymbol{F}^{\mathrm{T}} = \boldsymbol{F}\frac{\partial}{\partial t}[\underbrace{\boldsymbol{F}^{\mathrm{p}^{-1}}\bar{\mathbf{G}}^{-1}\boldsymbol{F}^{\mathrm{p}^{-\mathrm{T}}}}_{=0 \text{ (elastic process)}}]\boldsymbol{F}^{\mathrm{T}} = 0 \tag{22}$$

By the same token, no change in plastic deformation for the states remaining in the interior of the elastic domain also implies that the hardening variable and the plastic entropy would not be affected either, i.e.

$$\dot{\xi} = 0; \quad \dot{\eta}^{\mathrm{p}} = 0 \tag{23}$$

Taking into account that no dissipation would thus take place for an elastic material, along with the results in Eqs. (22) and (23), allows us to rewrite Eq. (21) as

$$0 = \mathscr{D}^{\mathrm{e}} := \left(\boldsymbol{\tau} - 2\frac{\partial\psi}{\partial\mathbf{g}}\right)\cdot\mathbf{d} + \left(-\eta^{\mathrm{e}} - \frac{\partial\psi}{\partial\theta}\right)\dot{\theta} \tag{24}$$

Finally, for independent values of $\mathbf{d}$ and $\dot{\theta}$ we can then conclude that

$$\boldsymbol{\tau} = 2\frac{\partial\psi}{\partial\mathbf{g}} \tag{25}$$

$$\eta^{\mathrm{e}} = -\frac{\partial\psi}{\partial\theta} \tag{26}$$

which represent the constitutive equations for the Kirchhoff stress tensor and the elastic entropy. If one assumes that the same constitutive equations remain valid for a plastic process where internal state variables do change, we can then arrive at the corresponding reduced form of the plastic dissipation

$$0 < \mathscr{D}^{\mathrm{p}} := -\frac{\partial \psi}{\partial \mathbf{b}^{\mathrm{e}}} \cdot L_v[\mathbf{b}^{\mathrm{e}}] + q\dot{\xi} + \theta\dot{\eta}^{\mathrm{p}} \tag{27}$$

where flux-like hardening variable is defined through its constitutive equation

$$q = -\frac{\partial \psi}{\partial \xi} \tag{28}$$

The key result for further reducing this inequality goes back to Ibrahimbegovic (1994), where it was shown that

$$\frac{\partial \psi}{\partial \mathbf{b}^{\mathrm{e}}} = \mathbf{g}\frac{\partial \psi}{\partial \mathbf{g}}\mathbf{b}^{\mathrm{e}^{-1}} \tag{29}$$

The latter can be proved by making use of the invariant form of the free energy in Eq. (11), the chain rule and the results that can be obtained by computing the directional derivatives of the eigenvalue problem in Eq. (6) leading to

$$\frac{\partial \lambda_i^{\mathrm{e}}}{\partial \mathbf{g}} = \frac{\lambda_i^{\mathrm{e}}}{2}\mathbf{g}^{-1}\boldsymbol{v}_i \otimes \mathbf{g}^{-1}\boldsymbol{v}_i \tag{30}$$

and

$$\frac{\partial \lambda_i^{\mathrm{e}}}{\partial \mathbf{b}^{\mathrm{e}}} = \frac{1}{2\lambda_i^{\mathrm{e}}}\boldsymbol{v}_i \otimes \boldsymbol{v}_i \tag{31}$$

In view of the Kirchhoff stress constitutive equation in Eq. (25), we can rewrite the reduced dissipation inequality for a plastic process, given in Eq. (27), by making use of the key result in Eq. (29) in the following form

$$0 < \mathscr{D}^{\mathrm{p}} = -\boldsymbol{\tau} \cdot \tfrac{1}{2}\mathbf{g}L_v[\mathbf{b}^{\mathrm{e}}]\mathbf{b}^{\mathrm{e}^{-1}} + q\dot{\xi} + \theta\dot{\eta}^{\mathrm{p}} \tag{32a}$$

It is interesting to note that the first two terms in Eq. (32a) above are identical to the dissipation of the plasticity model with no thermodynamical coupling; Therefore we refer to it as the mechanical dissipation

$$\mathscr{D}_{\mathrm{mech}} = -\boldsymbol{\tau} \cdot \tfrac{1}{2}\mathbf{g}L_v[\mathbf{b}^{\mathrm{e}}]\mathbf{b}^{\mathrm{e}^{-1}} + q\dot{\xi} \tag{32b}$$

and the remaining term in Eq. (32a) we thus call the thermal dissipation

$$\mathscr{D}_{\mathrm{ther}} = \theta\dot{\eta}^{\mathrm{p}} \tag{32c}$$

We further recall that when dealing with a plastic process, all the admissible states must verify the yield criterion $\phi(\boldsymbol{\tau}, \mathbf{g}, q, \theta) = 0$. The actual state which is selected is the one rendering the plastic dissipation maximum, which amounts to a thermomechanical generalization of the principle of maximum plastic dissipation (e.g. see Hill (1950, p. 60) or Lubliner (1984)). This principle can be set as a constrained minimization problem by resorting to the classical method of Lagrange multipliers (e.g. see Strang (1986, p. 729))

$$\min_{\tau^*, q^*, \theta^*} \max_{\gamma^*} \{\mathscr{L}^{\mathrm{p}}(\boldsymbol{\tau}^*, \bar{\mathbf{g}}, q^*, \theta^*, \gamma^*) = -\mathscr{D}^{\mathrm{p}}(\boldsymbol{\tau}^*, \bar{\mathbf{g}}, q^*, \theta^*) + \dot{\gamma}^*\phi(\boldsymbol{\tau}^*, \bar{\mathbf{g}}, q^*, \theta^*)\} \tag{33}$$

where $\dot{\gamma}^* > 0$ is the Lagrange multiplier. By taking into account the exact form of $\mathscr{D}^{\mathrm{p}}$ in Eq. (32a), the optimality condition for the Lagrangian above can be written as (e.g. see Strang (1986, p. 729)) according to

$$0 = \left.\frac{\partial \mathscr{L}^{\mathrm{p}}}{\partial \boldsymbol{\tau}^*}\right|_{\boldsymbol{\tau}} \quad \Rightarrow \quad L_v[\mathbf{b}^{\mathrm{e}}] = -2\dot{\gamma}\mathbf{g}^{-1}\frac{\partial \phi}{\partial \boldsymbol{\tau}}\mathbf{b}^{\mathrm{e}} \tag{34}$$

$$0 = \left.\frac{\partial \mathscr{L}^{\mathrm{p}}}{\partial q^*}\right|_q \Rightarrow \dot{\xi} = \dot{\gamma}\frac{\partial \phi}{\partial q} \tag{35}$$

and

$$0 = \left.\frac{\partial \mathscr{L}^{\mathrm{p}}}{\partial \theta^*}\right|_\theta \Rightarrow \dot{\eta}^{\mathrm{p}} = \dot{\gamma}\frac{\partial \phi}{\partial \theta} \tag{36}$$

which represent the evolution equations for internal variables in a plastic process, where $\phi(\cdot) = 0$. If one also assumes that $\dot{\gamma}$ would take zero value for an elastic process, where $\phi(\cdot) < 0$, we can define Eqs. (34)–(36) to apply for both elastic and plastic processes, supplemented by the corresponding Kuhn–Tucker format of loading/unloading conditions, differentiating between elastic and plastic processes with

$$\dot{\gamma} \geqslant 0; \quad \phi(\cdot) \leqslant 0; \quad \dot{\gamma}\phi(\cdot) = 0 \tag{37}$$

Remark 1. An alternative manner to solve the constrained minimization problem in Eq. (33) is by resorting to the penalty method by accepting a stress state outside the plastically admissible domain with $\phi(\cdot) > 0$, but attaching the corresponding penalty term to it. This can be formally presented as unconstrained minimization problem with

$$\min_{\tau^*, q^*, \theta^*} \{\mathscr{L}^{\mathrm{vp}}(\boldsymbol{\tau}^*, \bar{\mathbf{g}}, q^*, \theta^*) = -\mathscr{D}^{\mathrm{p}}(\boldsymbol{\tau}^*, \bar{\mathbf{g}}, q^*, \theta^*) + \mathscr{P}(\phi(\boldsymbol{\tau}^*, \bar{\mathbf{g}}, q^*, \theta^*))\}; \quad \mathscr{P}(\phi) := \begin{cases} 1/2\eta[\phi]^2; & \phi > 0 \\ 0; & \phi \leqslant 0 \end{cases} \tag{38}$$

where η is the penalty parameter. It is easy to see that the optimality conditions of such a problem can formally be written as those in Eqs. (34)–(36) if the plastic multiplier is computed with

$$\dot{\gamma} = \frac{\langle \phi \rangle}{\eta}; \quad \langle \phi \rangle := \begin{cases} \phi; & \phi > 0 \\ 0; & \phi \leqslant 0 \end{cases} \tag{39}$$

The penalty formulation of this kind can also be interpreted as the viscoplastic regularization (capable of accounting for rate effects) and η as the viscosity parameter.

Remark 2. In concluding this section we note that a number of tensorial equations developed in the foregoing can be simplified to appropriate scalar form when recast in principal axes. For example, by exploiting the invariant form of the free energy in Eq. (11) and the result in Eq. (30), we can rewrite the stress constitutive equations in Eq. (25) as

$$\boldsymbol{\tau} = \sum_{i=1}^{3} \underbrace{\lambda_i^{\mathrm{e}} \frac{\partial \tilde{\psi}(\lambda_i^{\mathrm{e}}, \theta)}{\partial \lambda_i^{\mathrm{e}}}}_{\tau_i} \mathbf{g}^{-1}\boldsymbol{v}_i \otimes \mathbf{g}^{-1}\boldsymbol{v}_i \tag{40}$$

The last result indicates that once the eigenvalue problem in Eq. (6) is solved for the corresponding principal covectors, the stress tensor computation would reduce to mere scalar computation of the principal values given as the partial derivatives of the invariant form of the free energy.

Similarly, by making use of the result $\partial\tau_i/\partial\boldsymbol{\tau} = \sum_{i=1}^{3} \boldsymbol{v}_i \otimes \boldsymbol{v}_i$ and the invariant form of the yield criterion in Eq. (13), the evolution equation in Eq. (34) can be rewritten as

$$L_v[\mathbf{b}^{\mathrm{e}}] = -2\dot{\gamma}\left(\sum_{i=1}^{3} \frac{\partial \phi}{\partial \tau_i} \mathbf{g}^{-1}\boldsymbol{v}_i \otimes \mathbf{g}^{-1}\boldsymbol{v}_i\right)\mathbf{b}^{\mathrm{e}} \tag{41}$$

2.3. Strong and weak forms of equilibrium and energy conservation equations

In the preceding section the standard thermodynamics considerations have furnished the constitutive equations for the dependent variables: the Kirchhoff stress $\boldsymbol{\tau}$, elastic entropy η^{e} and flux-like hardening variable q, given in Eqs. (25), (26) and (28), respectively. We have also shown that the principle of maximum plastic dissipation can be used to derive the evolution equation of internal variables: the left Cauchy–Green elastic deformation tensor $\mathbf{b}^{\mathrm{e}}$ in Eq. (34), hardening variable ξ in Eq. (35) and plastic entropy in Eq. (36). The coupled thermoplasticity model description is completed in this section by deriving the governing equation for two remaining state variables, the metric tensor $\mathbf{g}$ and the temperature θ. The latter is represented by the equilibrium (or momentum balance) equation and energy conservation equation, respectively. We first present the strong (or local) forms of these equations and then develop the corresponding weak forms.

To that end we first recall that the metric tensor $\mathbf{g}$ can be replaced in computation by the point mapping $\boldsymbol{\varphi}(\boldsymbol{x})$, which defines the deformed configuration, since the matrix representation of the metric tensor can be obtained as

$$g_{ij} = \boldsymbol{\varphi}_{,i} \cdot \boldsymbol{\varphi}_{,j} \tag{42}$$

where $(\cdot)_{,i}$ denotes the partial derivative with respect to the chosen coordinates. We also recall that the point mapping defines the components of the deformation gradient as

$$\boldsymbol{F} = [\boldsymbol{\varphi}_{,1}\boldsymbol{\varphi}_{,2}\boldsymbol{\varphi}_{,3}] \tag{43}$$

In developing the (linear) momentum balance equation we employ the Kirchhoff stress description and develop the local or strong form of the balance equation with respect to the initial configuration. In doing so, we first assume that the balance of mass enforced at the outset by imposing that $\partial\rho_0/\partial t \equiv 0$, where ρ_0 is the density in the initial configuration, and that the angular momentum balance would reduce to the condition of symmetry for the Kirchhoff stress tensor $\boldsymbol{\tau} = \boldsymbol{\tau}^{\mathrm{T}}$.

The linear momentum balance equation can than be written as

$$\mathrm{div}[\boldsymbol{\tau}\boldsymbol{F}^{-\mathrm{T}}] + \mathbf{f} = 0 \tag{44}$$

where $\mathrm{div}[\cdot]$ is the divergence operator with respect to the coordinates in the initial configuration. By multiplying the strong form of the equilibrium equation in Eq. (44) by a virtual velocity $\mathbf{w}$, and integrating by parts we can obtain the weak form of the last equation as

$$G_{\mathrm{M}}(\mathbf{g}, \mathbf{b}^{\mathrm{e}}, \xi, \theta, \mathbf{w}) = \int_{\mathscr{B}} \left(\frac{1}{2} L_w[\mathbf{g}] \cdot \boldsymbol{\tau} - \mathbf{w} \cdot \mathbf{f} \right) \mathrm{d}V + \int_{\partial\mathscr{B}} \mathbf{w} \cdot \bar{\mathbf{t}}\, \mathrm{d}A = 0 \tag{45a}$$

$$G_{\mathrm{T}}(\mathbf{g}, \mathbf{b}^{\mathrm{e}}, \xi, \theta, \vartheta) := \int_{\mathscr{B}} \{\vartheta[\theta\dot{\eta}^{\mathrm{e}} - \mathscr{D}_{\mathrm{mech}} - r] + k\nabla^{\varphi}\vartheta \cdot \nabla^{\varphi}\theta\}\, \mathrm{d}V + \int_{\partial\mathscr{B}} \vartheta\bar{q}\, \mathrm{d}A = 0 \tag{45b}$$

where $L_w[\mathbf{g}]$ it the Lie derivative driven by the virtual displacement, which can be written as

$$\begin{aligned} L_w[\mathbf{g}] &= \boldsymbol{F}^{-\mathrm{T}} \frac{\partial}{\partial t} [\boldsymbol{F}_{\epsilon}^{\mathrm{T}} \mathbf{g} \boldsymbol{F}_{\epsilon}] \boldsymbol{F}^{-1}; \quad \boldsymbol{F}_{\epsilon} = \nabla(\epsilon\mathbf{w}) + \boldsymbol{F} \\ &= \mathbf{g}\nabla^{\varphi}\mathbf{w} + (\nabla^{\varphi}\mathbf{w})^{\mathrm{T}}\mathbf{g}; \quad \nabla^{\varphi} = \boldsymbol{F}^{-\mathrm{T}}\nabla \end{aligned} \tag{46}$$

We note in passing that the weak form of the equilibrium equations in Eq. (45a) above is a function of all state variables, such a dependence being imposed through the constitutive equation for the Kirchhoff stress in Eq. (25).

Following the same line of developments, the energy conservation equation can first be written in the strong form with respect to the initial configuration

$$\dot{e} = \boldsymbol{\tau} \cdot \mathbf{d} - \mathrm{div}[\boldsymbol{F}^{-1}\mathbf{q}] + r \tag{47}$$

where r is the external heat source, and the Piola transformation is employed to reduce the second term to the material form, i.e.

$$J\,\mathrm{div}^{\varphi}(\mathbf{q}/J) = \mathrm{div}(\boldsymbol{F}^{-1}\mathbf{q}) \tag{48}$$

By appealing to the result on Eq. (17), we can rewrite the energy balance equation by accounting for dissipated energy as

$$-\mathrm{div}[\boldsymbol{F}^{-1}\mathbf{q}] + r = \theta\dot{\eta} - \mathscr{D} = \theta(\dot{\eta}^{\mathrm{e}} + \dot{\eta}^{\mathrm{p}}) - \mathscr{D} = \theta\dot{\eta}^{\mathrm{e}} - \mathscr{D}_{\mathrm{mech}} \tag{49}$$

where $\mathscr{D}_{\mathrm{mech}}$ was defined in first term of Eq. (32a). Then, the last equation can be rewritten as

$$\theta\dot{\eta}^{\mathrm{e}} = \mathscr{D}_{\mathrm{mech}} - J\,\mathrm{div}^{\varphi}(\mathbf{q}/J) + r \tag{50}$$

Moreover, if the Fourier law in Eq. (16) is chosen to govern the heat flux (the later assumption being consistent with the isotropy), we recover from Eq. (50) above the standard format of the strong form for nonstationary heat transfer equation.

The weak form of the energy equation can be obtained by multiplying Eq. (50) with the virtual temperature ϑ and integrating over the domain, and by making use of the integration by parts to reduce the order of derivative on the real temperature field to get Eq. (45b).

We note that Eq. (45b) provides a very suitable form of the energy equation from the standpoint of the subsequent numerical implementation, where the key role is played by the constitutive equation for elastic entropy in Eq. (26).

2.4. Model problem: von Mises thermoplasticity yield criterion and strain energy in logarithmic stretches

In this section we select a particular form of the yield criterion for the model problem quite typical for majority of metals and alloys corresponding to the von Mises thermoplasticity, and carry out the corresponding simplifications. The von Mises type yield criterion for finite deformation thermoplasticity can be written in terms of deviatoric part of the Kirchhoff stress tensor

$$\phi(\boldsymbol{\tau}, \mathbf{g}, q, \theta) := ||\mathrm{dev}_g[\boldsymbol{\tau}]|| - \sqrt{\frac{2}{3}}(\sigma_y(\theta) - q(\xi, \theta)) \leqslant 0 \tag{51}$$

where

$$\mathrm{dev}_g[\boldsymbol{\tau}] = \boldsymbol{\tau} - \tfrac{1}{3}(\boldsymbol{\tau} \cdot \mathbf{g})\mathbf{g}^{-1} \tag{52}$$

The same criterion can also be expressed in terms of the principal values of the Kirchhoff stress as

$$\phi(\tau_i, q, \theta) := \sqrt{\frac{2}{3}}(\tau_1^2 + \tau_2^2 + \tau_3^2 - \tau_1\tau_2 - \tau_2\tau_3 - \tau_3\tau_1)^{1/2} - \sqrt{\frac{2}{3}}(\sigma_y(\theta) - q(\xi, \theta)) \leqslant 0 \tag{53}$$

It is easy to see that the von Mises criterion in Eq. (53) is pressure insensitive leading to

$$\sum_{i=1}^{3} \frac{\partial\phi}{\partial\tau_i} = 0 \tag{54}$$

which further implies that the no plastic volume change would take place. The latter can be easily shown by making of the result in Eq. (1), from where it follows that $J = J^{\mathrm{e}}J^{\mathrm{p}}$, with $J^{\mathrm{e}} = \lambda_1^{\mathrm{e}}\lambda_2^{\mathrm{e}}\lambda_3^{\mathrm{e}}$. By exploiting the results in Eqs. (7), (31) and (41), we can easily show that

$$\frac{\partial J^{\mathrm{e}}}{\partial \mathbf{b}^{\mathrm{e}}} \cdot L_v[\mathbf{b}^{\mathrm{e}}] = -J^{\mathrm{e}}\dot{\gamma}\sum_{i=1}^{3}\frac{\partial \phi}{\partial \tau_i} = 0 \tag{55}$$

which further implies that $J^{\mathrm{e}} = J^{\mathrm{e}}\mathbf{g}^{-1}\cdot\mathbf{d}$, and thus that all the change of volume is elastic, which leaves $J^{\mathrm{p}} = 1$.

Another important result that comes as a consequence of using the von Mises yield criterion concerns a corresponding simplification that one can bring to the expression for the mechanical dissipation in Eq. (32b). Namely, it follows from Eqs. (51) and (35) that

$$\begin{aligned}\mathscr{D}_{\mathrm{mech}} &= -\boldsymbol{\tau}\cdot\tfrac{1}{2}\mathbf{g}L_v[\mathbf{b}^{\mathrm{e}}]\mathbf{b}^{\mathrm{e}^{-1}} + q\dot{\xi} \\ &= \dot{\gamma}\left(\sum_{i=1}^{3}\tau_i\frac{\partial\phi}{\tau_i} + \sqrt{\frac{2}{3}}q\right) = \dot{\gamma}\left[\sqrt{\frac{2}{3}}(\tau_1^2+\tau_2^2+\tau_3^2-\tau_1\tau_2-\tau_2\tau_3-\tau_3\tau_1)^{1/2} + \sqrt{\frac{2}{3}}q\right]\end{aligned} \tag{56}$$

By taking into account the given form of the yield criterion in Eq. (53) it then follows that the mechanical dissipation can be reduced to a very simple form

$$\mathscr{D}_{\mathrm{mech}} = \sqrt{\frac{2}{3}}\dot{\gamma}\sigma_y(\theta) \tag{57}$$

which can be used to further simplify the form of the energy balance equation in Eqs. (50) and (45b). The hardening variable $q(\xi,\theta)$ is assumed to be a combination of linear and saturation-type hardening with

$$q := -\{[\sigma_\infty(\theta)-\sigma_y(\theta)][1-\exp(-\beta\xi)] + H(\theta)\xi\} \tag{58}$$

where

$$\begin{aligned}\sigma_y(\theta) &= \sigma_y(\theta_0)[1-\omega(\theta-\theta_0)] \\ \sigma_\infty(\theta) &= \sigma_\infty(\theta_0)[1-\omega(\theta-\theta_0)] \\ H(\theta) &= H(\theta_0)[1-\omega(\theta-\theta_0)]\end{aligned} \tag{59}$$

where $\sigma_y(\theta_0)$ is the initial yield stress, $\sigma_\infty(\theta_0)$ the final saturation hardening stress, $H(\theta_0)$ is the linear hardening modulus, all obtained at the reference temperature θ_0. The description of the hardening model has to be completed by choosing the saturation coefficient β and the temperature coefficient ω.

With these results in hand we can also compute a simplified form of the evolution equation for plastic entropy in Eq. (36) to get

$$\dot{\eta}^{\mathrm{p}} = \dot{\gamma}\sqrt{\frac{2}{3}}\frac{\partial}{\partial\theta}[\sigma_y(\theta)-q(\xi,\theta)] = -\dot{\gamma}\sqrt{\frac{2}{3}}\omega[\sigma_y(\theta_0)-q(\xi,\theta_0)] \tag{60}$$

Replacing this result in second term of Eq. (32a) we can compute the thermal dissipation as

$$\mathscr{D}_{\mathrm{ther}} = -\dot{\gamma}\sqrt{\frac{2}{3}}\theta\omega[\sigma_y(\theta_0)-q(\xi,\theta_0)] \tag{61}$$

Thus it follows that $\mathscr{D}_{\mathrm{ther}} \geqslant 0$ for positive value of constant ω, which, in view of the result in Eq. (59) implies that the yield surface contracts with increasing temperature, or, in other words, induces the thermoplastic softening which is in accordance with experimental results (see Lubliner (1987)).

We also choose a specific model for the strain energy given in terms of the elastic principal stretches, hardening variable and the temperature according to

$$\psi(\lambda_i^{\mathrm{e}},\xi,\theta) = \hat{\psi}(\lambda_i^{\mathrm{e}}) + \chi(\xi,\theta) + M(J^{\mathrm{e}},\theta) + T(\theta) \tag{62}$$

In Eq. (62) we choose $\hat{\psi}(\cdot)$ as a quadratic form of elastic principal stretches

$$\hat{\psi}(\lambda_i^{\mathrm{e}}) = \tfrac{1}{2}\lambda(\ln\lambda_1^{\mathrm{e}} + \ln\lambda_2^{\mathrm{e}} + \ln\lambda_3^{\mathrm{e}})^2 + \mu[(\ln\lambda_1^{\mathrm{e}})^2 + (\ln\lambda_2^{\mathrm{e}})^2 + (\ln\lambda_3^{\mathrm{e}})^2] \tag{63}$$

with λ and μ as the Lamé coefficients. Moreover, $\chi(\xi,\theta)$ is chosen such to recover the hardening description given as $q = -\partial\chi/\partial\xi$.

The thermomechanical coupling is governed by the choice of the function $M(\cdot)$ in Eq. (62); By generalizing the corresponding choice from the linear theory (e.g. see Carlson (1972)) we choose a form that couples only volumetric elastic deformation with the thermal effects through

$$M(J^{\mathrm{e}},\theta) = -3\alpha(\lambda + \tfrac{2}{3}\mu)(\theta - \theta_0)(\ln J^{\mathrm{e}})/J^{\mathrm{e}} \tag{64}$$

where α is the coefficient of thermal expansion. Finally, we can choose the form of $T(\cdot)$ such that the only coefficient that remains to be specified is the heat capacity constant c, with

$$T(\theta) = c[(\theta - \theta_0) - \theta\ln(\theta/\theta_0)] \tag{65}$$

Namely, it is easy to see that with such a choice, the left hand side of the strong form of the energy balance equation in Eq. (50) reduces to a constant value, since

$$-\theta\frac{\partial^2\psi}{\partial\theta^2} \equiv -\theta\frac{\partial^2 T(\theta)}{\partial\theta^2} = c \tag{66}$$

Given this form of the strain energy, the stress constitutive equation in Eq. (40) can be rewritten as

$$\boldsymbol{\tau} = 2\frac{\partial\hat{\psi}}{\partial\lambda_i^{\mathrm{e}}}\frac{\partial\lambda_i^{\mathrm{e}}}{\partial\mathbf{g}} + 2\frac{\partial M}{\partial J^{\mathrm{e}}}\frac{\partial J^{\mathrm{e}}}{\partial\mathbf{g}} = \sum_{i=1}^{3}\underbrace{\lambda_i^{\mathrm{e}}\frac{\partial\hat{\psi}}{\partial\lambda_i^{\mathrm{e}}}}_{\hat{\tau}_i}\mathbf{g}^{-1}\boldsymbol{v}_i\otimes\mathbf{g}^{-1}\boldsymbol{v}_i + \underbrace{2\frac{\partial M}{\partial J^{\mathrm{e}}}\tfrac{1}{2}J^{\mathrm{e}}}_{p}\mathbf{g}^{-1} \tag{67}$$

where $\hat{\tau}_i$ are the corresponding contributions from the mechanical part $\hat{\psi}(\cdot)$ in Eq. (62) towards the total values of principal stresses, which can be written as

$$\hat{\tau}_i = (\lambda + 2\mu)(\ln\lambda_i^{\mathrm{e}}) + \lambda(\ln\lambda_j^{\mathrm{e}} + \ln\lambda_k^{\mathrm{e}}), \quad i = 1,2,3,\ \ j = 2,3,1,\ \ k = 3,1,2 \tag{68}$$

whereas p is the coupling term, pressure-like stress contribution which can be obtained from Eq. (64) as

$$p = -3\alpha(\lambda + \tfrac{2}{3}\mu)(\theta - \theta_0)\frac{1 - \ln J^{\mathrm{e}}}{J^{\mathrm{e}}} \tag{69}$$

The constitutive equation for elastic entropy in Eq. (26) can also be simplified in accordance with the strain energy chosen in Eq. (62) as

$$\begin{aligned}\eta^{\mathrm{e}} &= -\frac{\partial M}{\partial\theta} - \frac{\partial T}{\partial\theta} - \frac{\partial\chi}{\partial\theta} \\ &= 3\alpha(\lambda + \tfrac{2}{3}\mu)(\ln J^{\mathrm{e}})/J^{\mathrm{e}} + c\ln(\theta/\theta_0) + [\sigma_\infty(\theta_0)\omega - \sigma_y(\theta_0)\omega]\left[\xi + \frac{1}{\beta}\exp(-\beta\xi)\right] + \tfrac{1}{2}H(\theta_0)\omega\xi^2\end{aligned} \tag{70}$$

2.5. Consistent linearization of the weak form—Mechanical part

The weak form of the mechanical equilibrium equations can be written as

$$G_{\mathrm{M}}(\boldsymbol{\varphi},\mathbf{b}^{\mathrm{e}},\xi,\theta,\mathbf{w}) = \int_{\mathscr{B}}\left(\boldsymbol{\tau}\cdot\frac{1}{2}L_w[\mathbf{g}]\right)\mathrm{d}V - G_{\mathrm{ext}} = 0 \tag{71}$$

The consistent linearization of the first term in Eq. (71) above, the so-called stress divergence term, gives rise to the corresponding part of the tangent operator, which can be written as

$$DG_{\mathrm{M_{int}}} = \mathbf{K}_{\mathrm{MM_{geom}}}(\mathbf{w},\mathbf{u}) + \mathbf{K}_{\mathrm{MM_{mat}}}(\mathbf{w},\mathbf{u}) + \mathbf{K}_{\mathrm{MT_{mat}}}(\mathbf{w},\upsilon) \tag{72}$$

where $\mathbf{u}$ is the incremental displacement field and υ is the incremental temperature field. The first two terms in Eq. (72) above are identical to the tangent operator obtained for the purely mechanical case (see Ibrahimbegovic and Gharzeddine (1998)), i.e.

$$\mathbf{K}_{\mathrm{MM_{mat}}}(\mathbf{w},\mathbf{u}) = \int_{\mathscr{B}} \frac{1}{2} L_w[\mathbf{g}] : 2\frac{\partial \boldsymbol{\tau}}{\partial \mathbf{g}} : \frac{1}{2} L_u[\mathbf{g}]\, \mathrm{d}V \tag{73}$$

and

$$\mathbf{K}_{\mathrm{MM_{geom}}}(\mathbf{w},\mathbf{u}) = \int_{\mathscr{B}} \frac{1}{2} L_u[L_w[\mathbf{g}]] : \boldsymbol{\tau}\, \mathrm{d}V \tag{74}$$

where $L_w[\mathbf{g}]$ is already defined in Eq. (46), whereas

$$L_u[\mathbf{g}] = \mathbf{g}\nabla^{\varphi}\mathbf{u} + (\nabla^{\varphi}\mathbf{u})^{\mathrm{T}}\mathbf{g} \tag{75}$$

and

$$L_u[L_w[\mathbf{g}]] = \boldsymbol{F}^{-\mathrm{T}} \frac{\partial}{\partial t}[\boldsymbol{F}_{\epsilon}^{\mathrm{T}} L_w[\mathbf{g}] \boldsymbol{F}_{\epsilon}] \boldsymbol{F}^{-1} = [\mathbf{g}\nabla^{\varphi}\mathbf{w} + (\nabla^{\varphi}\mathbf{w})^{\mathrm{T}}\mathbf{g}]\nabla^{\varphi}\mathbf{u} + (\nabla^{\varphi}\mathbf{u})^{\mathrm{T}}[\mathbf{g}\nabla^{\varphi}\mathbf{w} + (\nabla^{\varphi}\mathbf{w})^{\mathrm{T}}\mathbf{g}] \tag{76}$$

The only term which pertains to the present elastoplastic case is the elastoplastic modulus in Eq. (73), given as $2(\partial\boldsymbol{\tau}/\partial\mathbf{g})$, which will be presented explicitly in the next section.

The last term in Eq. (72) represents the thermomechanical coupling part of the tangent operator (due to temperature dependence of material properties), which can be written as

$$\mathbf{K}_{\mathrm{MT_{mat}}}(\mathbf{w},\upsilon) = \int_{\mathscr{B}} \frac{\partial \boldsymbol{\tau}}{\partial \theta} \cdot \frac{1}{2} L_w[\mathbf{g}]\upsilon\, \mathrm{d}V \tag{77}$$

where the Kirchhoff stress derivative with respect to temperature can be written as

$$\mathbf{C}^{\mathrm{p}}_{\mathrm{MT}} := \frac{\partial \boldsymbol{\tau}}{\partial \theta} = -3\alpha\left(\lambda + \tfrac{2}{3}\mu\right) \frac{1 - \ln J^{\mathrm{e}}}{J^{\mathrm{e}}} \mathbf{g}^{-1} \tag{78}$$

2.6. Consistent linearization of the weak form—Thermal part

The weak form of the energy balance equation can be written as

$$G_{\mathrm{T}}(\boldsymbol{\varphi}, \mathbf{b}^{\mathrm{e}}, \xi, \theta, \vartheta) = \int_{\mathscr{B}} \{\vartheta[\theta(\eta^{\mathrm{e}} - \eta^{\mathrm{e}}_n)/\Delta t - \mathscr{D}_{\mathrm{mech}}] - k\nabla^{\varphi}\vartheta \cdot \nabla^{\varphi}\theta\}\, \mathrm{d}V - \int_{\mathscr{B}} \vartheta r\, \mathrm{d}V - \int_{\partial\mathscr{B}} \vartheta \bar{q}\, \mathrm{d}A = 0 \tag{79}$$

where η^{e} is already defined in Eq. (70), and η^{e}_n is the corresponding value in the previous increment.

The consistent linearization is again carried out with respect to both displacement and temperature leading to the following form of the tangent operator

$$DG_{\mathrm{T_{int}}} = \mathbf{K}_{\mathrm{TM_{geom}}}(\vartheta,\mathbf{u}) + \mathbf{K}_{\mathrm{TM_{mat}}}(\vartheta,\mathbf{u}) + \mathbf{K}_{\mathrm{TT_{mat}}}(\vartheta,\upsilon) \tag{80}$$

The first two terms in Eq. (80) above arise due to thermomechanical coupling (i.e. heat flux which is influenced by deformation, or structural dissipative term). The first of the two term defines the geometric part of the coupling tangent operator can be written as (see Ibrahimbegovic et al. (2001))

$$\mathbf{K}_{\mathrm{TM_{geom}}}(\vartheta,\mathbf{u}) = \int_{\mathscr{B}} L_u[\nabla^{\varphi}\vartheta] \cdot \mathbf{q}\, \mathrm{d}V \tag{81}$$

where

$$L_u[\nabla^{\varphi}\vartheta] = \nabla^{\varphi}\vartheta\nabla^{\varphi}\mathbf{u} + (\nabla^{\varphi}\mathbf{u})^{\mathrm{T}}\nabla^{\varphi}\vartheta \tag{82}$$

The material part of the same operator can be written as

$$\mathbf{K}_{\mathrm{TM}_{\mathrm{mat}}}(\vartheta,\mathbf{u}) = \int_{\mathscr{B}} \vartheta 2\,\partial_{\mathbf{g}}\eta^{\mathrm{e}} \cdot \frac{1}{2}L_u[\mathbf{g}]\,\frac{\theta}{\Delta t}\,\mathrm{d}V + \int_{\mathscr{B}} -\vartheta 2\,\partial_{\mathbf{g}}\mathscr{D}_{\mathrm{mech}} \cdot \frac{1}{2}L_u[\mathbf{g}]\,\mathrm{d}V \tag{83}$$

with

$$2\partial_{\mathbf{g}}\eta^{\mathrm{e}} = 2\frac{\partial\eta^{\mathrm{e}}}{\partial J^{\mathrm{e}}}\frac{\partial J^{\mathrm{e}}}{\partial\mathbf{g}} = 2\frac{\partial M}{\partial J^{\mathrm{e}}}\tfrac{1}{2}J^{\mathrm{e}}\mathbf{g}^{-1} = p\mathbf{g}^{-1} \tag{84}$$

and

$$C^{\mathrm{p}}_{\mathrm{TM}} = 2\,\partial_{\mathbf{g}}\mathscr{D}_{\mathrm{mech}} = \sqrt{\frac{2}{3}}\frac{1}{\Delta t}\mathbf{D}^{\mathrm{tp}} : \mathbf{n} \tag{85}$$

The purely thermic part of the tangent operator can be written as

$$\mathbf{K}_{\mathrm{TT}_{\mathrm{mat}}}(\vartheta,\upsilon) = \int_{\mathscr{B}} \left\{ \upsilon\left[\frac{1}{\Delta t}((\eta^{\mathrm{e}} - \eta^{\mathrm{e}}_n) + \theta\partial_{\theta}\eta^{\mathrm{e}}) - \partial_{\theta}\mathscr{D}_{\mathrm{mech}}\right]\vartheta - \nabla^{\varphi}\upsilon \cdot k\nabla^{\varphi}\vartheta \right\}\mathrm{d}V \tag{86}$$

where, by making use of the result in Eq. (60), we can write

$$C^{\mathrm{p}}_{\mathrm{TT}} = \partial_{\theta}\left[\sqrt{\frac{2}{3}}\dot{\gamma}\sigma_y(\theta)\right] \tag{87}$$

$$C^{\mathrm{p}}_{\mathrm{TT}} = \left[\sqrt{\frac{2}{3}}\Delta\gamma\sigma_{y,\theta} - \frac{\sigma_{y,\theta} + \chi_{,\xi\theta}}{3\mu}\right]\Big/\Delta t \tag{88}$$

and

$$\partial_{\theta}\eta^{\mathrm{e}} = -T_{,\theta\theta}(\theta) \tag{89}$$

2.7. Tangent elastoplastic modulus

Tangent elastoplastic modulus, which is defined through the Kirchhoff stress tensor derivative with respect to metric tensor

$$\mathbf{D}^{\mathrm{tp}}_{n+1} = 2\frac{\partial\boldsymbol{\tau}}{\partial\mathbf{g}}\bigg|_{n+1} \tag{90}$$

In deriving the last result one ought to take into account the principal axis representation of the Kirchhoff stress tensor

$$\boldsymbol{\tau} = \sum_{i=1}^{3}\hat{\tau}_i\mathbf{g}^{-1}\boldsymbol{v}_i \otimes \mathbf{g}^{-1}\boldsymbol{v}_i + p\mathbf{g}^{-1} \tag{91}$$

where $\hat{\tau}_i$ and p are already defined by Eqs. (68) and (69), respectively. With this result on hand, the tangent modulus can be written as

$$\mathbf{D}^{\mathrm{tp}}_{n+1} = 2\frac{\partial\boldsymbol{\tau}}{\partial\mathbf{g}}\bigg|_{n+1} = \sum_{i=1}^{3}2\frac{\partial\hat{\tau}_i}{\partial\mathbf{g}}\mathbf{g}^{-1}\boldsymbol{v}_i \otimes \mathbf{g}^{-1}\boldsymbol{v}_i + \sum_{i=1}^{3}2\hat{\tau}_i\frac{\partial}{\partial\mathbf{g}}[\mathbf{g}^{-1}\boldsymbol{v}_i \otimes \mathbf{g}^{-1}\boldsymbol{v}_i] + 2\frac{\partial p}{\partial\mathbf{g}}\mathbf{g}^{-1} + 2p\frac{\partial\mathbf{g}^{-1}}{\mathbf{g}} \tag{92}$$

with

$$\frac{\partial p}{\partial \mathbf{g}} = \frac{\partial p}{\partial J^{\mathrm{e}}}\frac{\partial J^{\mathrm{e}}}{\partial \mathbf{g}} = \frac{\partial p}{\partial J^{\mathrm{e}}} J^{\mathrm{e}} \mathbf{g}^{-1}; \quad \frac{\partial \mathbf{g}^{-1}}{\partial \mathbf{g}} = \mathbf{I}_{\mathbf{g}^{-1}} \tag{93}$$

The explicit form of the elastoplastic tangent operator can finally be written as the superposition of the mechanical part and thermal part (for details, see Ibrahimbegovic and Gharzeddine (1998))

$$\mathbf{D}^{\mathrm{tp}}_{n+1} = \underbrace{\mathbf{D}^{\mathrm{ep}}_{\mathrm{mat}} + \mathbf{D}^{\mathrm{ep}}_{\mathrm{geom}}}_{\text{classical plasticity}} + \frac{\partial p}{\partial J^{\mathrm{e}}} J^{\mathrm{e}} \mathbf{g}^{-1} \otimes \mathbf{g}^{-1} + 2p\mathbf{I}_{\mathbf{g}^{-1}} \tag{94}$$

with

$$\mathbf{D}^{\mathrm{ep}}_{\mathrm{mat}} = \sum_{i=1}^{3}\sum_{j=1}^{3} \mathbf{C}^{\mathrm{ep}}_{ij} (\mathbf{g}^{-1}\boldsymbol{v}_i \otimes \mathbf{g}^{-1}\boldsymbol{v}_i) \otimes (\mathbf{g}^{-1}\boldsymbol{v}_i \otimes \mathbf{g}^{-1}\boldsymbol{v}_i) \tag{95}$$

and

$$\begin{aligned}\mathbf{D}^{\mathrm{ep}}_{\mathrm{geom}} = \sum_{i=1}^{3} \frac{2\tau_i}{d_i} \{ & \mathbf{I}_{b^{\mathrm{e}}} - \mathbf{b}^{\mathrm{e}} \otimes \mathbf{b}^{\mathrm{e}} - I_3 \lambda_i^2 [\mathbf{I}_{g^{-1}} + (\mathbf{g}^{-1} - \mathbf{g}^{-1}\boldsymbol{v}_i \otimes \mathbf{g}^{-1}\boldsymbol{v}_i) \otimes (\mathbf{g}^{-1} - \mathbf{g}^{-1}\boldsymbol{v}_i \otimes \mathbf{g}^{-1}\boldsymbol{v}_i)] \\ & + (\lambda_i^{\mathrm{e}})^2 [(\mathbf{g}^{-1}\boldsymbol{v}_i \otimes \mathbf{g}^{-1}\boldsymbol{v}_i) \otimes \mathbf{b}^{\mathrm{e}} + \mathbf{b}^{\mathrm{e}} \otimes (\mathbf{g}^{-1}\boldsymbol{v}_i \otimes \mathbf{g}^{-1}\boldsymbol{v}_i) + (\mathbf{I}_1 - 4(\lambda_i^{\mathrm{e}})^2)(\mathbf{g}^{-1}\boldsymbol{v}_i \otimes \mathbf{g}^{-1}\boldsymbol{v}_i) \otimes (\mathbf{g}^{-1}\boldsymbol{v}_i \otimes \mathbf{g}^{-1}\boldsymbol{v}_i)]\}\end{aligned} \tag{96}$$

where

$$d_i = ((\lambda_j^{\mathrm{e}})^2 - (\lambda_i^{\mathrm{e}})^2)((\lambda_k^{\mathrm{e}})^2 - (\lambda_i^{\mathrm{e}})^2), \quad i = 1,2,3, \quad j = 1 + \mathrm{mod}(3,i), \quad k = 1 + \mathrm{mod}(3,k)$$

$$[\mathbf{I}_{b^{\mathrm{e}}}]^{ijkl} = \tfrac{1}{2}(b^{\mathrm{e},ik}b^{\mathrm{e},jl} + b^{\mathrm{e},il}b^{\mathrm{e},k}); \qquad [\mathbf{I}_{g^{-1}}]^{ijkl} = -\tfrac{1}{2}(g^{ik}g^{jl} + g^{il}g^{jk})$$

2.8. Method of incompatible modes in finite deformation thermoplasticity

In extending the method of incompatible modes, which was shown to perform well for finite deformation plasticity (e.g. see Ibrahimbegovic and Gharzeddine (1998)), to the present fully coupled thermomechanical case, the standard form of the deformation gradient $\boldsymbol{F} = \nabla\boldsymbol{\varphi}$ is replaced by an enhanced form

$$\tilde{\boldsymbol{F}} = [\mathbf{I} + \mathbf{a}_{\mathrm{M}}]\boldsymbol{F} \tag{97}$$

where $(\mathbf{I} + \mathbf{a}_{\mathrm{M}})$ is the spatial deformation gradient superposed onto the compatible part. It is convenient to construct the former starting from the material gradient $\mathbf{A}_{\mathrm{M}}$ of an imaginary incompatible displacement field $\boldsymbol{\alpha}_{\mathrm{M}}$ (see Ibrahimbegovic and Frey (1993)), i.e.

$$\mathbf{a}_{\mathrm{M}} = \mathbf{A}_{\mathrm{M}}\boldsymbol{F}^{-1} = \nabla\boldsymbol{\alpha}_{\mathrm{M}}\boldsymbol{F}^{-1} \tag{98}$$

The latter forces us to include the incompatible displacement gradient among the state variables. The weak form of the equilibrium equation can be rewritten as

$$G_{\mathrm{M}}(\tilde{\boldsymbol{\varphi}}, \mathbf{A}_{\mathrm{M}}, \mathbf{b}^{\mathrm{e}}, \xi, \tilde{\theta}, \mathbf{w}) := \int_{\mathscr{B}} \boldsymbol{\tau} : \frac{1}{2}[\mathbf{g}\nabla^{\tilde{\varphi}}\mathbf{w} + (\nabla^{\tilde{\varphi}}\mathbf{w})^{\mathrm{T}}\mathbf{g}]\,\mathrm{d}V - G_{\mathrm{ext}} = 0 \tag{99}$$

where $\nabla^{\tilde{\varphi}}\mathbf{w} = \nabla\mathbf{w}\tilde{\boldsymbol{F}}^{-1}$. In this case, however, the weak form in Eq. (99) is not complete without taking into account the corresponding variation of the incompatible modes, which gives rise to a complementary term

$$G_{\mathrm{M}}(\tilde{\boldsymbol{\varphi}}, \mathbf{A}_{\mathrm{M}}, \mathbf{b}^{\mathrm{e}}, \xi, \tilde{\theta}, \boldsymbol{\zeta}_{\mathrm{M}}) := \int_{\mathscr{B}} \boldsymbol{\tau} : \frac{1}{2}[\mathbf{g}\nabla^{\tilde{\varphi}}\boldsymbol{\zeta}_{\mathrm{M}} + (\nabla^{\tilde{\varphi}}\boldsymbol{\zeta}_{\mathrm{M}})^{\mathrm{T}}\mathbf{g}]\,\mathrm{d}V = 0 \tag{100}$$

where $\nabla^{\tilde{\varphi}}\boldsymbol{\zeta}_{\mathrm{M}} = \nabla\boldsymbol{\zeta}_{\mathrm{M}}\tilde{\boldsymbol{F}}^{-1}$. In the same manner, the energy balance equation can be rewritten as

$$G_{\mathrm{T}}(\tilde{\boldsymbol{\varphi}}, \mathbf{A}_{\mathrm{M}}, \mathbf{b}^{\mathrm{e}}, \xi, \tilde{\theta}, \vartheta) = \int_{\mathscr{B}} \{\vartheta[c(\tilde{\theta} - \tilde{\theta}_n)/\Delta t - \mathscr{D}_{\mathrm{mech}}] - k\nabla^{\tilde{\varphi}}\vartheta \cdot \nabla^{\tilde{\varphi}}\tilde{\theta}\}\,\mathrm{d}V - G_{\mathrm{ext}} = 0 \tag{101}$$

where $\nabla^{\tilde{\varphi}}\vartheta = \nabla\vartheta\tilde{\boldsymbol{F}}^{-1}$ and $\nabla^{\tilde{\varphi}}\tilde{\theta} = \nabla^{\tilde{\varphi}}\theta\tilde{\boldsymbol{F}}^{-1}$, which needs to be completed with

$$G_{\mathrm{T}}(\tilde{\boldsymbol{\varphi}}, \mathbf{A}_{\mathrm{M}}, \mathbf{b}^{\mathrm{e}}, \xi, \tilde{\theta}, \zeta_{\mathrm{T}}) = \int_{\mathscr{B}} \{\zeta_{\mathrm{T}}[c(\tilde{\theta} - \tilde{\theta}_n)/\Delta t - \mathscr{D}_{\mathrm{mech}}] - k\nabla^{\tilde{\varphi}}\zeta_{\mathrm{T}} \cdot \nabla^{\tilde{\varphi}}\tilde{\theta}\}\,\mathrm{d}V = 0 \tag{102}$$

where $\nabla^{\tilde{\varphi}}\zeta_{\mathrm{T}} = \nabla\zeta_{\mathrm{T}}\tilde{\boldsymbol{F}}^{-1}$.

The subsequent procedure of consistent linearization is performed in a very similar manner as in the previous case with no incompatible modes; Therefore, further details are outlined.

3. Numerical examples

In this section we present the results of several numerical simulations which further illustrate a very satisfying performance of the proposed methodology for fully coupled thermoplasticity. All the computations are performed by computer program FEAP, developed by Prof. R.L. Taylor at UC Berkeley (e.g. see Zienkiewicz and Taylor (1989)). We have developed and tested enhanced elements for both 2d and 3d problems, employing 4 or 8 nodes respectively and the corresponding set of incompatible modes. Both elements employ the principal axis methodology and the first-order backward Euler and exponential approximation schemes to carry out the plastic flow computation.

3.1. Thermoplastic cylinder under internal pressure

The first example is adapted from early work of Argyris and Doltsinis (1981) and later work of Simo and Miehe (1992) to test the developed solution scheme. The cylinder, with internal radius $a_0 = 100$ (mm) and external radius $b_0 = 200$ (mm), is considered as infinitely long. Therefore, only a 'slice' of thickness $h = 100$ (mm) is modeled by a mesh of 10 elements, with the boundary condition imposed on the displacement components along the cylinder axis set to zero, along with the corresponding heat flux. The external surface of the cylinder is maintained at the reference temperature $\theta_0 = 293$ (K), whereas the internal surface is submitted to the same temperature and pressure loading. The material properties of the cylinder, chosen to be the same as proposed earlier by Argyris and Doltsinis (1981) and Simo and Miehe (1992), combine elasto-plastic linear strain hardening and thermal softening models (see Table 1).

Table 1
Thermoplastic cylinder under internal pressure: material parameters

Bulk modulus	$\kappa = 58333$ N/mm^2
Shear modulus	$\mu = 26926$ N/mm^2
Density	$\rho = 2.7 \times 10^{-9}$ N s^2/mm^4
Yield stress	$\sigma_y = 70$ N/mm^2
Strain hardening modulus	$K_{\mathrm{iso}} = 210$ N/mm^2
Heat conductivity	$k = 150$ N/s K
Heat capacity	$c = 0.9 \times 10^9$ mm^2/s^2 K
Thermal expansion	$\alpha = 23.8 \times 10^{-6}$ K^{-1}
Thermal softening modulus	$\omega = 3 \times 10^{-4}$ K^{-1}

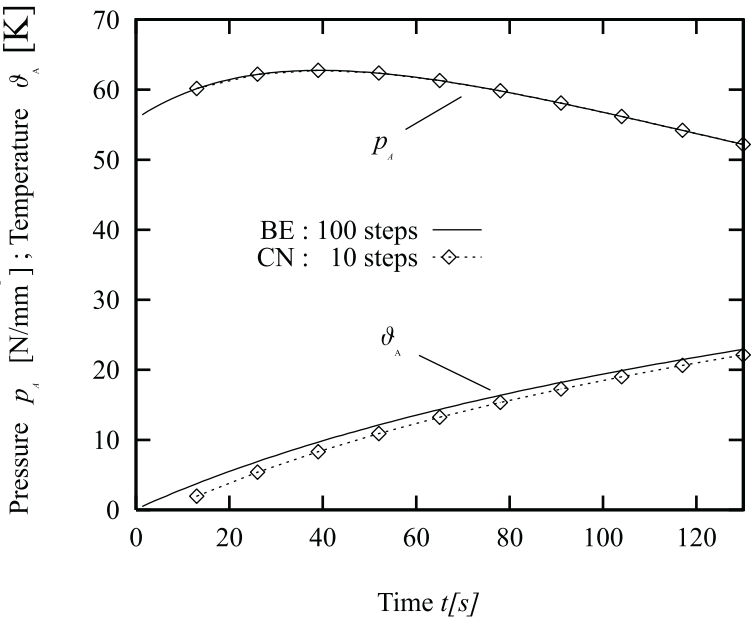

Fig. 1. Thermoplastic cylinder: internal pressure and relative temperature at internal surface.

In practical computation the internal pressure is replaced by the imposed displacement at the inner cylinder surface, which results with a very stable solution procedure. The imposed displacement is increased reaching the final value of the internal radius $a = 2.3\,a_0 = 230$ (mm), leading to clearly a very large deformation. At that level of deformation, the cylinder has crossed to the plastic regime and the plastic dissipation is much more dominant than the structural heating in the resulting thermomechanical exchange.

The resulting temporal variation of the internal pressure as presented in Fig. 1, matches quite well the previous results of Simo and Miehe (1992). We have also obtained the corresponding temperature variation at the inner surface of cylinder, by using the first-order backward Euler scheme and 100 time steps and the second-order Crank–Nicholson scheme (e.g. see Hughes (1987)) and 10 time steps. Those results, in rather good agreement with one another, are also presented in Fig. 1.

The second analysis of the same problem considers different values of the total time to apply the imposed displacement, such as $T \to 0$, 1, 5, 10, 30 and 100 (s). The corresponding spatial distribution of the temperature field in the final deformed configuration of the cylinder is given in Fig. 2. One can observe that increasing the values of the total time leads quite naturally to more evenly distributed temperature field (with the temperature field as constant for $T \to \infty$), due to a more significant diffusion process. We note in passing that the spatial distribution of the temperature field can be used to quantify the total plastic dissipation.

3.2. Strain localization problem

In this example we present a 2d and a 3d version of the strain localization problems, where the response of the structure is computed in the post-peak regime which requires the proper portion of viscosity (e.g. see Needleman (1988)) to produce a mesh-insensitive numerical result (see Ibrahimbegovic and Chorfi (2000)).

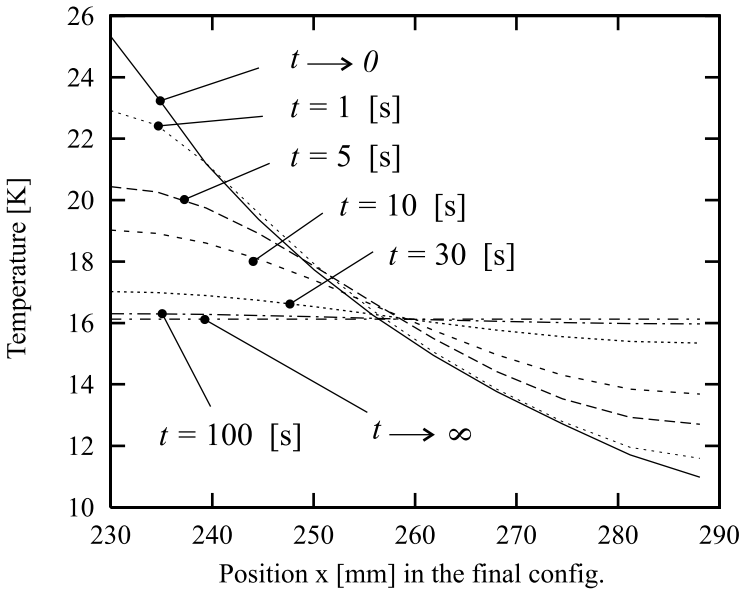

Fig. 2. Thermoplastic cylinder: spatial distribution of the temperature field in the final deformed configuration for different values of the total time.

3.2.1. Plane strain specimen in simple tension test

In this example we consider a rectangular specimen in plane strain submitted to uniform traction forces. The length of the specimen $l = 53.334$ (mm) and its width $b = 12.826$ (mm). The chosen values of the thermomechanical properties of the specimen are given in Table 2.

The analysis is performed under imposed displacement, keeping the corresponding temperature constant and equal to the reference temperature $\theta_0 = 293$ (K). The remaining displacement boundary condition are chosen to impose the symmetry for a quarter of the specimen which is used in the analysis, whereas the remaining temperature boundary conditions consider the isolated edges of the specimen (see Fig. 3).

The mesh grading, which is also presented in Fig. 3, is chosen such to better accommodate the shear band formation. We use in total 200 elements with 4 nodes and incompatible modes.

Table 2
Plane strain specimen: material properties

Bulk modulus	$\kappa = 164206$ N/mm^2
Shear modulus	$\mu = 801938$ N/mm^2
Density	$\rho = 7.8 \times 10^{-9}$ N s^2/mm^4
Yield stress	$\sigma_y = 450$ N/mm^2
Saturation stress	$\sigma_\infty = 715$ N/mm^2
Strain hardening modulus	$K_{\text{iso}} = 129.24$ N/mm^2
Hardening exponent	$\beta = 16.93$
Heat conductivity	$k = 45$ N/s K
Heat capacity	$c = 0.46 \times 10^9$ mm^2/s^2 K
Thermal expansion	$\alpha = 1 \times 10^{-5}$ K^{-1}
Thermal softening modulus	$\omega = 0.002$ K^{-1}

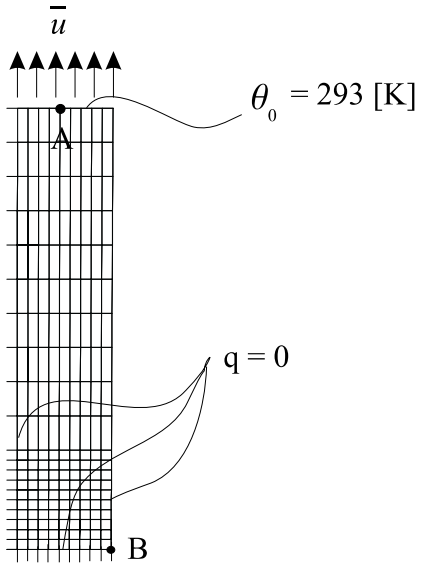

Fig. 3. Plane strain specimen: boundary conditions and mesh grading.

The total value of the imposed displacement is increased to $\bar{u} = 8$ (mm), with the rate of increase kept constant at $\dot{u} = 1$ (mm/s). The analysis is performed with a viscoplastic model using three different values of viscosity parameter $\eta = 10^{-3}$, $\eta = 50$ and $\eta = 10^{3}$ (s). The latter value of viscosity gives practically the same numerical result as the classical plasticity model. Such a conclusion applies for both the computed value of the total traction force, as presented in Fig. 4, and the temperature variation in the center of the specimen, as shown in Fig. 5.

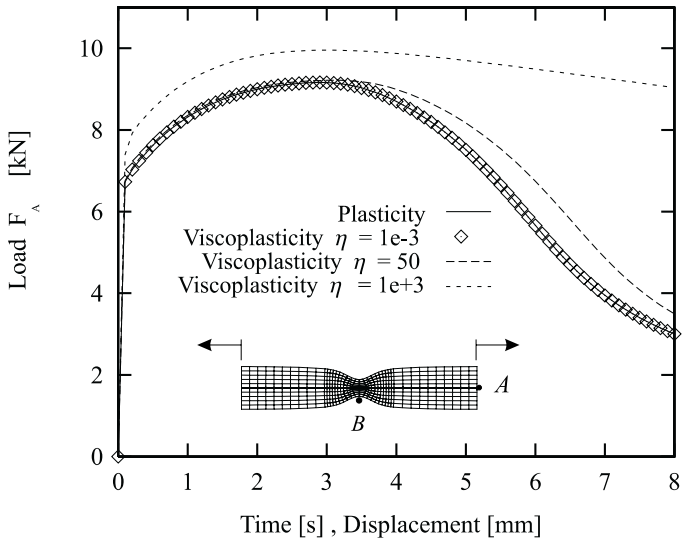

Fig. 4. Plane strain specimen: load–displacement diagram.

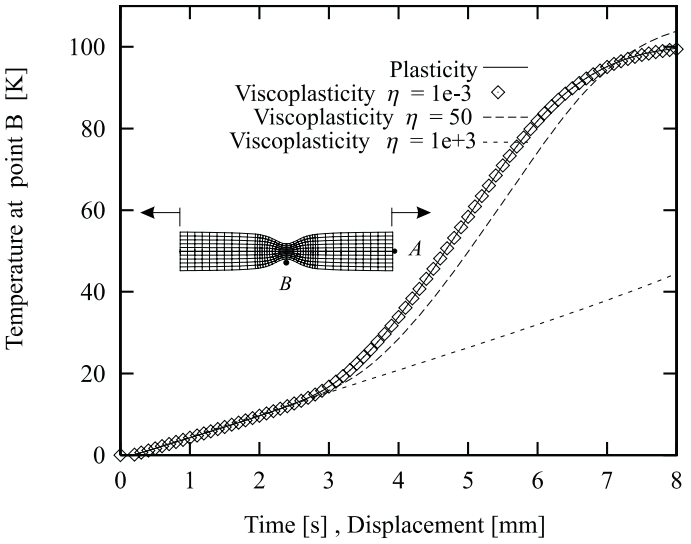

Fig. 5. Plane strain specimen: temperature temporel variation.

In Fig. 6 we present the initial configuration of the specimen and the deformed configuration obtain at time $t = 6$ (s) by either the viscoplasticity model (with $\eta = 50$) or the rate-independent plasticity model. The characteristic shear band localization patterns occur in a similar way for both models. The corresponding contours of the shear stress, as shown in Fig. 7 for both models, further reiterate the shear band formation as the precursor to fracture. We note that the shear band formation in this model of coupled thermoplasticity need not be triggered in an artificial manner (such as weakening of one of the elements) since it arises as a consequence of the thermal softening. As shown in Fig. 8, showing the contours of the temperature field, the most pronounced temperature increase is related to the strain localization zone.

The most prominent increase of shear band formation follow the classical inclination at 45° with respect to the vertical axis, for both plastic and viscoplastic model. This is confirmed by the results presented in Fig. 9, where the contours of the strain hardening variable (so-called equivalent plastic strain) are presented for three different values of imposed displacement at $\bar{u} = 4$, 5 or 6 (mm).

Additional analysis of thermomechanical coupling effective carried out for different rates of increase of the imposed displacement, considering the total time to reach the final value $\bar{u} = 8$ (mm) as $T = 8$, 12, 24, 36 or 100 (s). The corresponding temperature field distribution along the specimen axis is computed and the results are plotted in Fig. 10. We can note again that slower increase of the external load leaves more time to redistribute more evenly the temperature field.

3.2.2. Circular bar in a simple tension test

The same kind of analysis as the one presented in the previous example is then carried out for a circular bar. The length of the bar $l = 53.334$ (mm) and its radius $r = 6.413$ (mm). The material properties of the bar are selected identical to those used in the previous example and stated in Table 2. Due to symmetry, only one eighth of the bar is used in the analysis, with imposing the appropriate boundary conditions of displacements and temperature, the same as those indicated in Fig. 3. The finite element model employs in

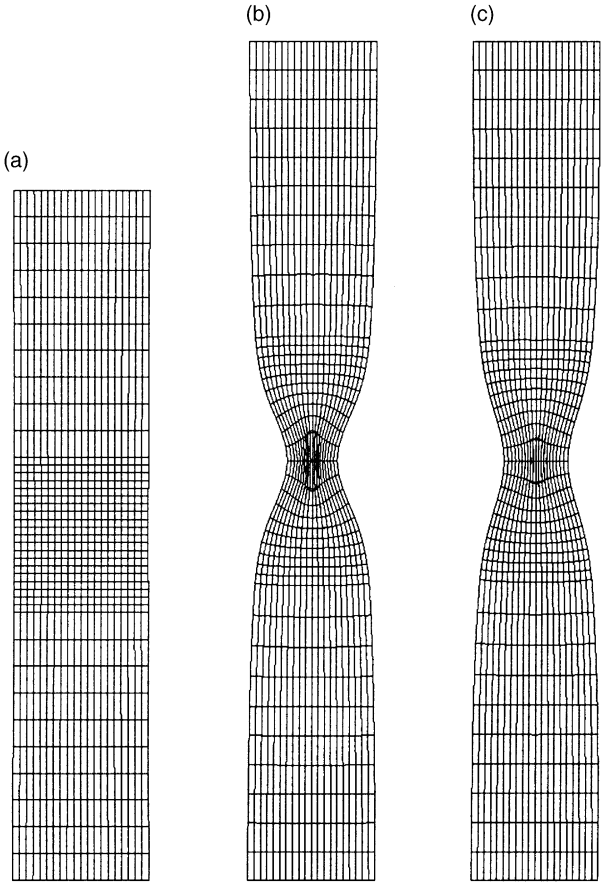

Fig. 6. Plane strain specimen: (a) initial mesh, (b) deformed mesh at $t = 6$ (s) for plastic model and (c) deformed mesh at $t = 6$ (s) for viscoplastic model.

total 960 8-node enhanced brick elements, and the corresponding mesh grading which takes into account the prospective localization zone is shown in Fig. 11.

The load–displacement diagram is computed for three different values of viscosity parameter, $\eta = 10^3$, 50 and 10^{-3}. As shown in Fig. 12, the latter result practically coincides with the one obtained for the rate-independent plasticity model. The time variation of the temperature in the center of the bar is given in Fig. 13.

Successive deformed shapes of the bar are shown in Fig. 14 indicating clearly the strain localization pattern, and the spatial temperature distribution, shown in Fig. 15, displays the plastic deformation induced heating in the central portion of the bar.

3.3. Cyclic loading on a thermoplastic plate

The last example concerns the cyclic loading analysis on a plate composed of viscoplastic material. The width of the plate is considered to be infinitely long to allow us to use the corresponding 2d plane strain model. The plate length is $l = 50$ (mm) and its thickness $t = 5$ (mm) and subjected to imposed vertical

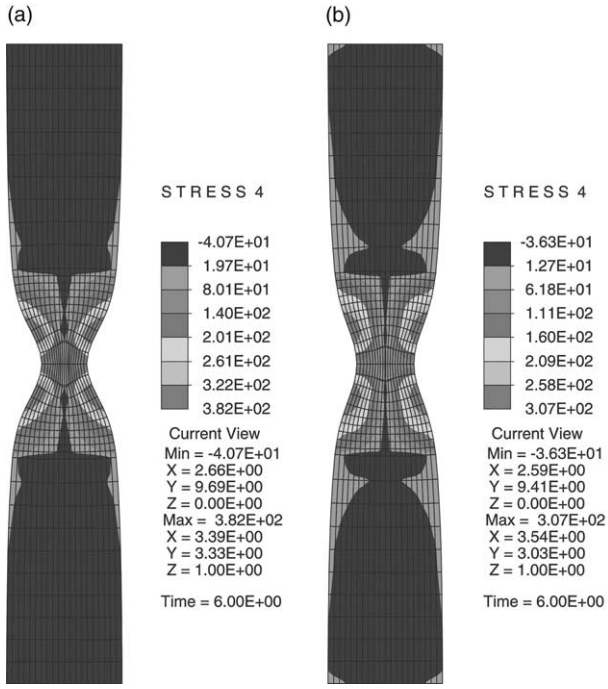

Fig. 7. Plane strain specimen: contours of shear stress at $t = 6$ (s), (a) plastic model and (b) viscoplastic model.

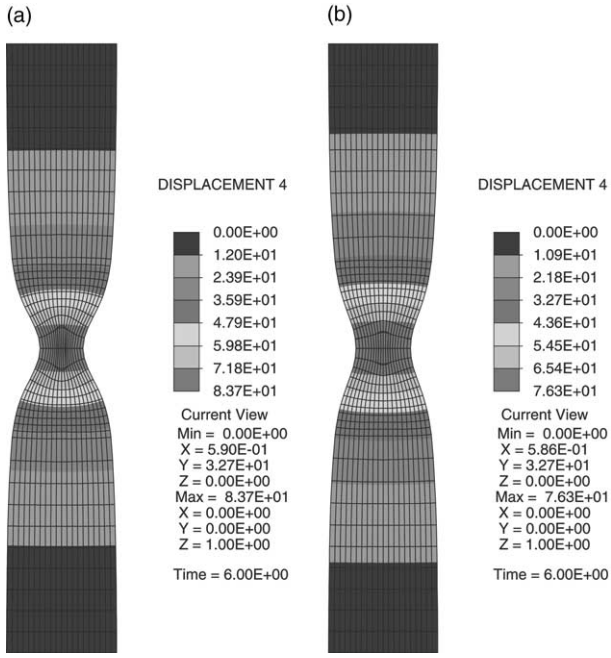

Fig. 8. Plane strain specimen: contours of temperature field at $t = 6$ (s), (a) plastic model and (b) viscoplastic model.

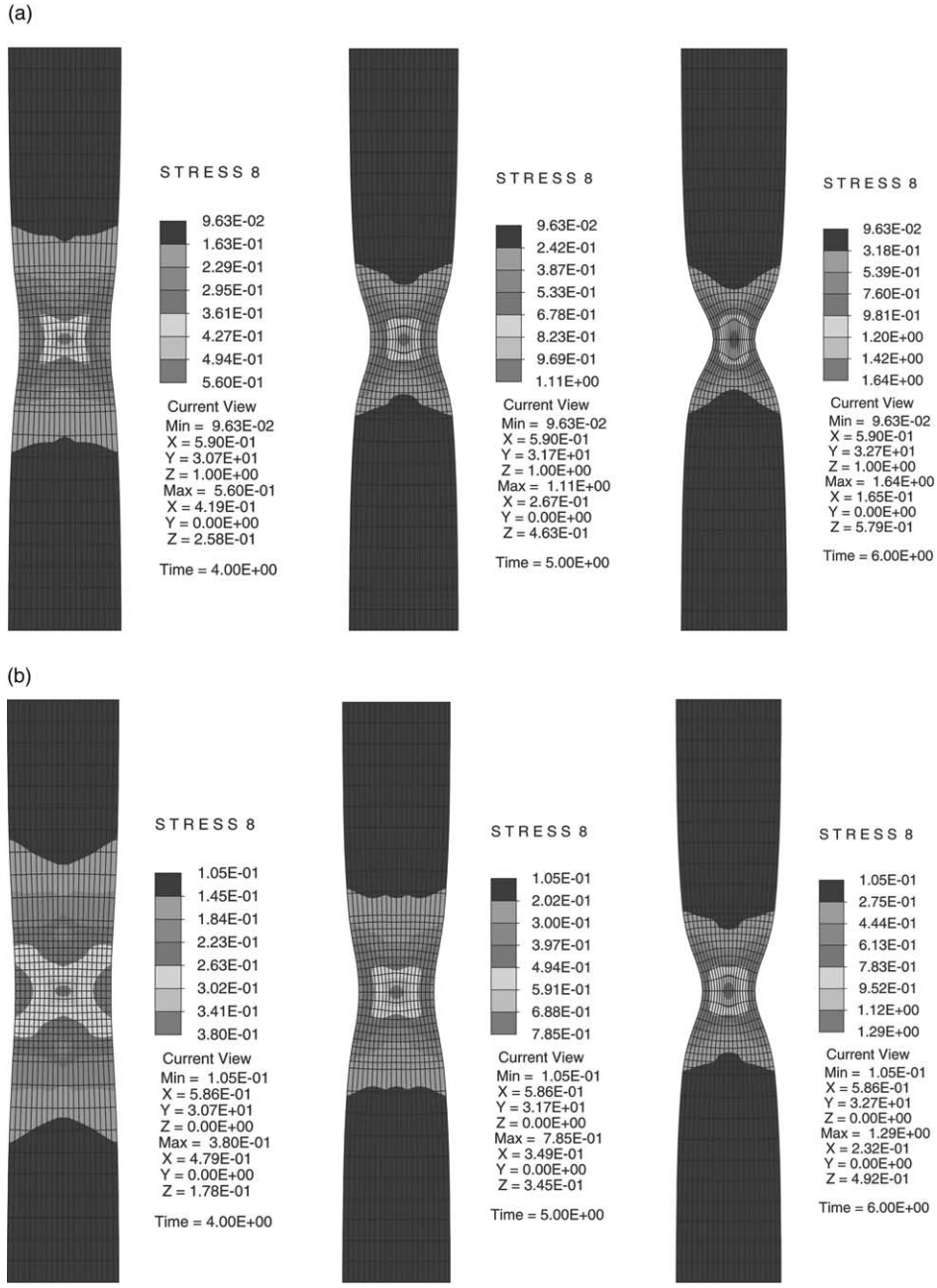

Fig. 9. Plane strain specimen: contours of strain hardening variable for plastic and viscoplastic model at $\bar{u} = 4$, 5 or 6 (mm).

displacement at other end, given as $u_b(t) = 5\sin(2\pi t)$ (mm). The finite element model of the plate constructed for half of the plate consists of 200 enhanced 4-node elements. It is shown in Fig. 16, along with the corresponding mechanical and thermal boundary conditions. The material properties of the plate are presented in Table 3.

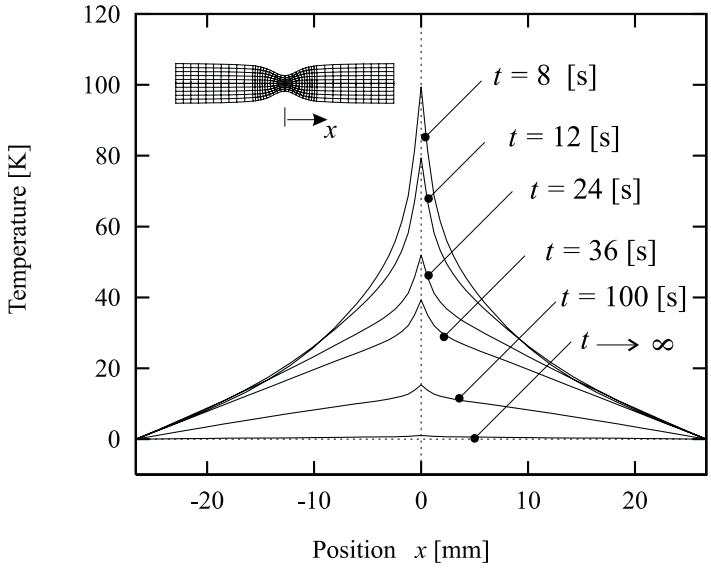

Fig. 10. Plane strain specimen: temperature field distribution in the final deformed configuration.

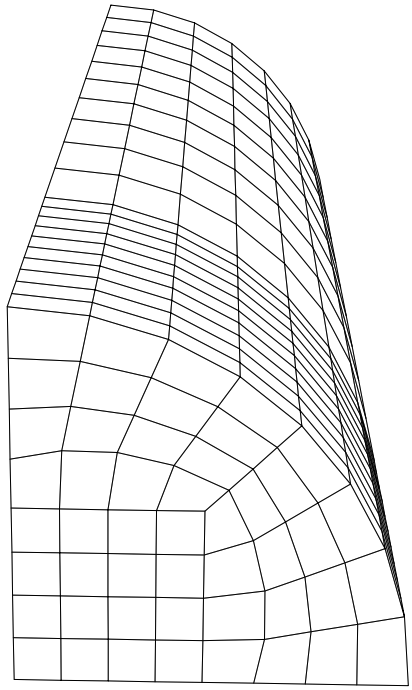

Fig. 11. Circular bar: finite element mesh.

We note that viscosity effect is considered, with $\eta = 10$, and the kinematic hardening (see Ibrahimbegovic and Chorfi (2000)) is introduced to better capture the Bauschinger effect for cyclic loading.

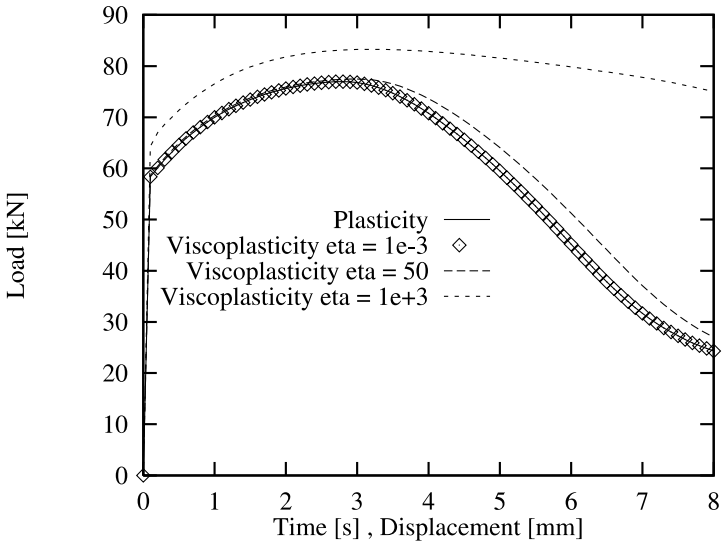

Fig. 12. Circular bar: load–displacement diagram.

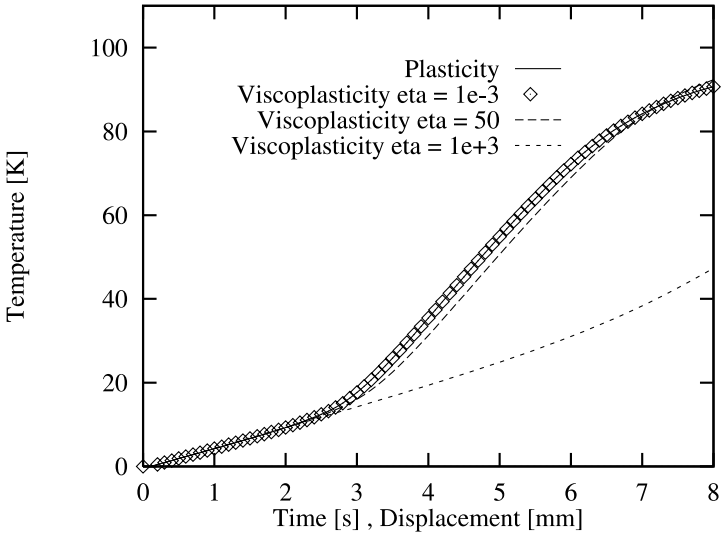

Fig. 13. Circular bar: temperature temporel variation.

The numerical analysis is performed with the time step $\Delta t = 0.01$. The loading at the free end of the plate induces the large plastic deformation in the central part of the plate, with characteristic strain localization patterns shown in Fig. 17. As shown in the same figure, these large plastic deformations are accompanied by a significant temperature increase due to thermomechanical coupling effects.

The time variation of the temperature at points A and C in the upper and lower surface in the center of the plate are represented in Fig. 18 and of the total loading in Fig. 19. We can see that both type of

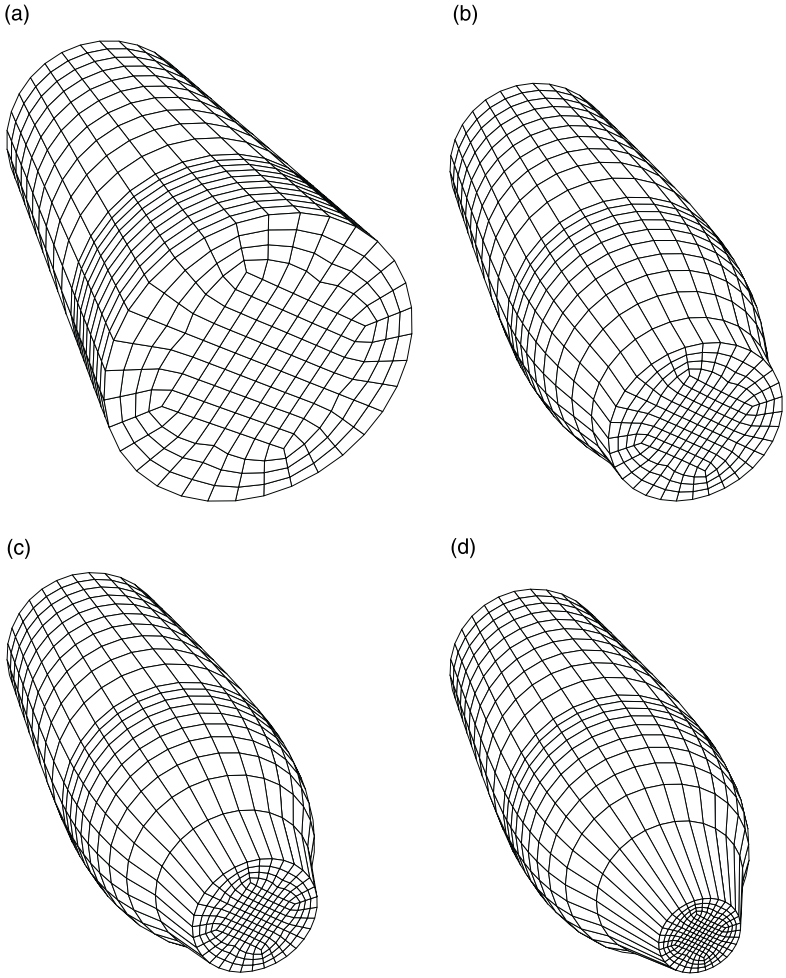

Fig. 14. Circular bar: deformed shapes at $t = 0$, 6, 7 and 8 (s).

equations keep increasing in time, which is in accordance with the well-known ratcheting effect for this kind of cyclic loading.

Finally, in order to illustrate the role of the rate of loading application in thermomechanical coupling we repeat the last analysis for the load increase rate which is 10 times larger, i.e. with $u_b(t) = 5 \sin\ (20\pi t)$ (mm). The corresponding time variation of temperature and the total loading are given in Figs. 20 and 21 respectively. We can see that the temperatures at points A and C increase more rapidly, since less time is left for heat diffusion effect; However, no significant change is noted in total load increase.

4. Conclusions

In this work we proposed an extension of the finite deformation plasticity model of Ibrahimbegovic (1994) to the case of fully coupled thermomechanical response. It was shown that the minimum number of

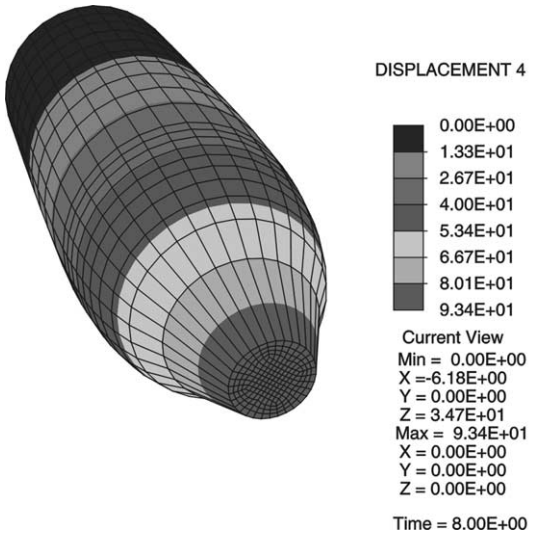

Fig. 15. Circular bar: temperature contours.

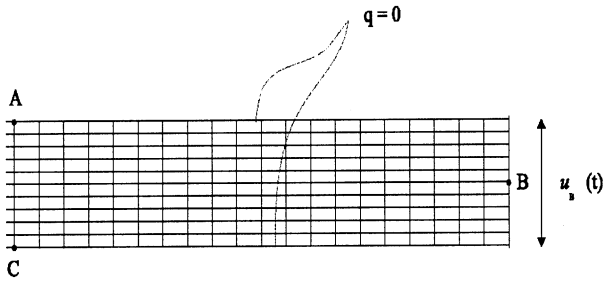

Fig. 16. Cyclic loading on a plate: FE mesh and boundary conditions.

Table 3
Cyclic loading on a plate: material properties

Bulk modulus	$\kappa = 58333\ \mathrm{N/mm^2}$
Shear modulus	$\mu = 26926\ \mathrm{N/mm^2}$
Density	$\rho = 2.7 \times 10^{-9}\ \mathrm{N\,s^2/mm^4}$
Saturation stress	$\sigma_y = 70\ \mathrm{N/mm^2}$
Isotropic hardening modulus	$K_{\mathrm{iso}} = 105\ \mathrm{N/mm^2}$
Kinematic hardening modulus	$K_{\mathrm{cin}} = 105\ \mathrm{N/mm^2}$
Viscosity parameter	$\eta = 10\ \mathrm{s}$
Heat conductivity	$k = 150\ \mathrm{N/s\,K}$
Heat capacity	$c = 0.9 \times 10^9\ \mathrm{mm^2/s^2\,K}$
Reference temperature	$\theta_0 = 293\ \mathrm{K}$
Thermal expansion	$\alpha = 23.8 \times 10^{-6}\ \mathrm{K^{-1}}$
Thermal softening modulus	$\omega = 3 \times 10^{-4}\ \mathrm{K^{-1}}$

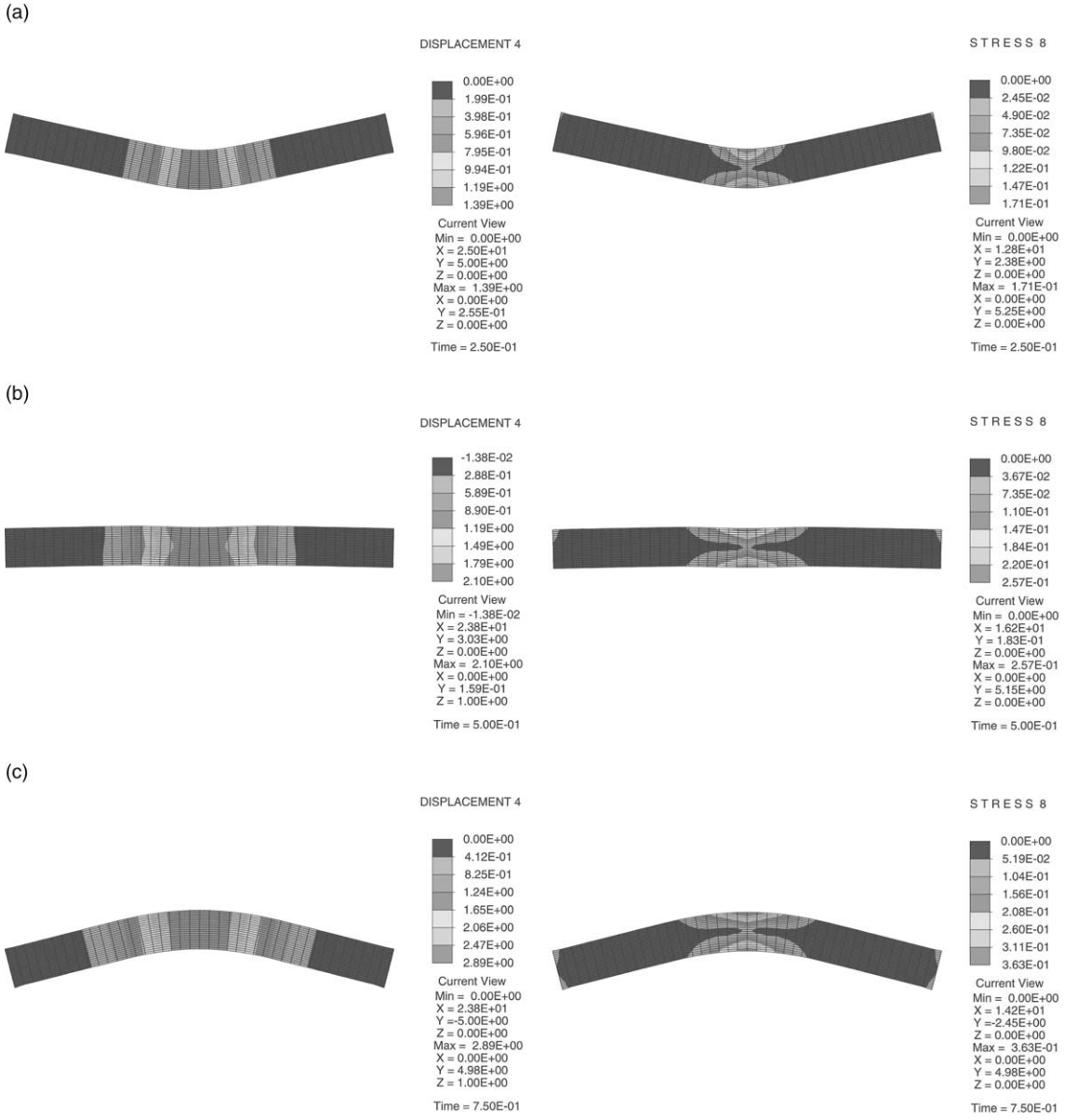

Fig. 17. Cyclic loading on a plate: contours of the temperature field and viscoplastic equivalent deformation at times (a) $t = 0.25$ (s), (b) $t = 0.5$ (s) and (c) $t = 0.75$ (s).

hypotheses, including the multiplicative decomposition of deformation gradient, the isotropy of elastic response and the generalization of the principle of maximum plastic dissipation to the thermomechanical setting, can be used to develop all the governing equations for such a model.

It is also shown how the principal axis methodology of Hill can be applied to significantly simplify both the theoretical formulation and numerical implementation for the model of this kind. In particular, the

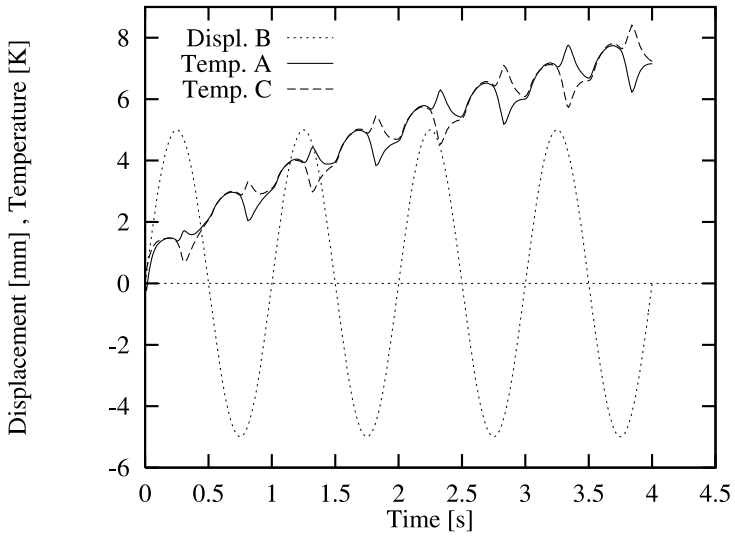

Fig. 18. Cyclic loading on a plate: time variation of temperature at point A and C.

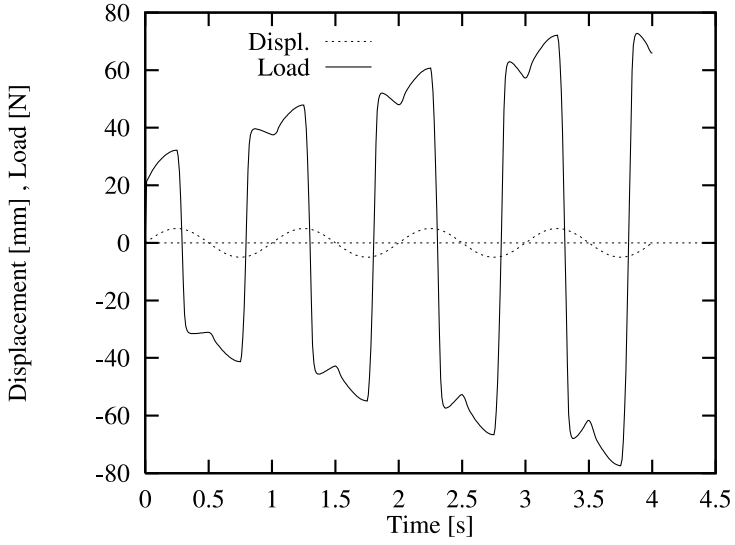

Fig. 19. Cyclic loading on a plate: time variation of loading at point B.

principal axis based numerical implementation of finite deformation plasticity, which seems to have already gained a universal acceptance in purely mechanical setting for the reason of its efficiency, has been extended by the present paper the setting of thermomechanics.

The model problem of deviatoric plasticity and thermomechanical coupling which concerns the volumetric response is developed in detail. Several numerical examples demonstrated the utility of the proposed

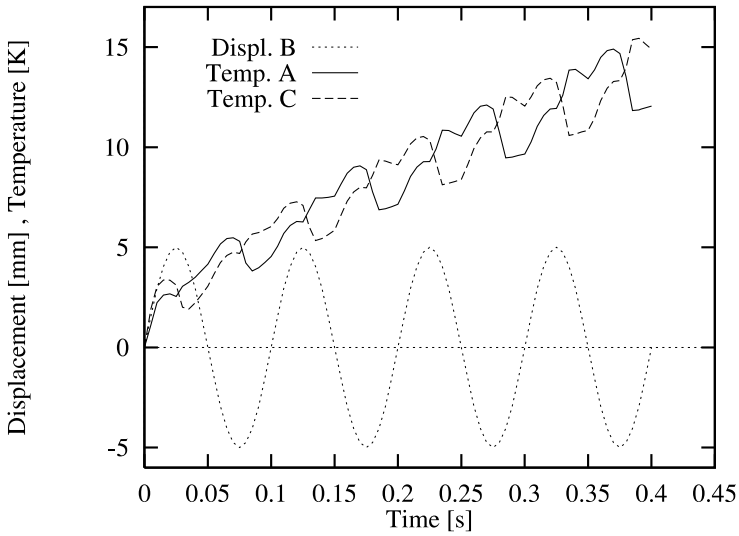

Fig. 20. Cyclic loading on a plate: time variation of temperature at point A and C.

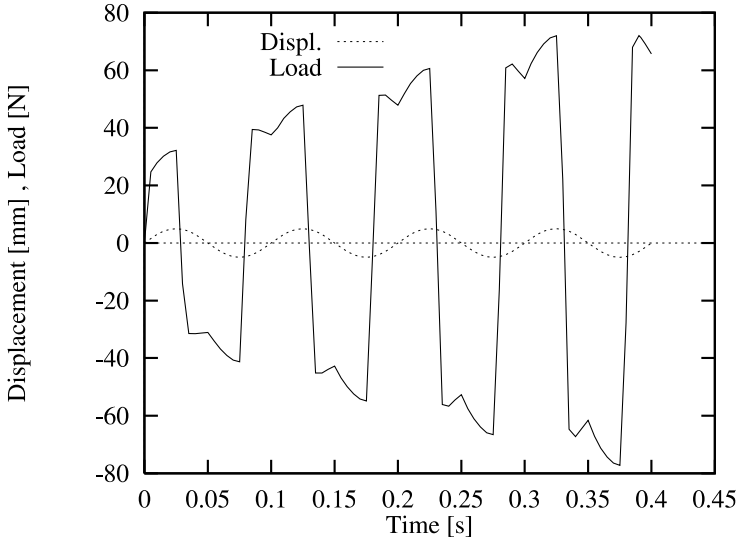

Fig. 21. Cyclic loading on a plate: time variation of loading at point B.

methodology in dealing with fully coupled thermomechanical analysis at large viscoplastic strains, as well as in capturing the localization phenomena and ratcheting effects for cyclic loading.

Acknowledgements

This work was supported by French and Algerian Ministries of Research and Education, by the Fund of Scientific and Technological Collaboration between France and Quebec and by a CNRS/LG2MS Grant. This support is gratefully acknowledged.

References

Argyris, J.H., St. Doltsinis, J., 1981. On the natural formulation and analysis of large deformation coupled thermomechanical problems. Comp. Methods Appl. Mech. Engng. 25, 195–253.

Argyris, J.H., St. Doltsinis, J., Pimenta, P.M., Wustenberg, H., 1982. Thermomechanical response of solids at high strains—natural approach. Comput. Methods Appl. Engng. 32, 3–57.

Armero, F., Simo, J.C., 1993. A priori stability estimates and unconditionally stable product formula algorithms for nonlinear coupled thermoplasticity. Int. J. Plasticity 9, 749–782.

Carlson, D.E., 1972. In: Linear Thermoelasticity, in Mechanics of Solids, vol. II. Springer, Berlin.

Cuitino, A., Ortiz, M., 1992. A material-independent method for extending stress update algorithms from small-strain plasticity to finite plasticity with multiplicative kinematics. Engng. Comput. 9, 437–451.

Drucker, D.C., 1988. Conventional and unconventional plastic response and representation. Appl. Mech. Rev. 41, 151–167.

Ericksen, J.L., 1998. Introduction to the Thermodynamics of Solids. Springer, Berlin.

Eterovic, A.L., Bathe, K.J., 1990. A hyperelastic-based large strain elasto-plastic constitutive formulation with combined isotropic-kinematic hardening using the logarithmic stress and strain measures. Int. J. Numer. Methods Engng. 30, 1099–1114.

Gurtin, M.E., 1981. An Introduction to Continuum Mechanics. Academic Press, New York.

Hill, R., 1950. The Mathematical Theory of Plasticity. Oxford University Press, London.

Hill, R., 1978. Aspects of invariance in solid mechanics. Adv. Appl. Mech. 18, 1–75.

Hughes, T.J.R., 1987. The Finite Element Method: Linear Static and Dynamic Analysis. Prentice Hall, Englewood Cliffs, NJ.

Ibrahimbegovic, A., 1994. Equivalent Eulerian and Lagrangian formulation of finite deformation elastoplasticity in principal axes. Int. J. Solids Struct. 31, 3027–3040.

Ibrahimbegovic, A., Chorfi, L., 2000. Viscoplasticity model at finite deformations with combined isotropic and kinematic hardening. Comput. Struct. 77, 509–525.

Ibrahimbegovic, A., Frey, F., 1993. Geometrically nonlinear method of incompatible modes in application to finite elasticity with finite rotation fiels. Int. J. Numer. Methods Engng. 36, 4185–4200.

Ibrahimbegovic, A., Gharzeddine, F., 1998. Finite deformation plasticity in principal axes: from a manifold to the Euclidean setting. Comput. Methods Appl. Mech. Engng. 171, 341–369.

Ibrahimbegovic, A., Chorfi, L., Gharzeddine, F., 2001. Thermomechanical coupling at finite elastic strain: covariant formulation and numerical implementation. Commun. Numer. Methods Engng. 17, 275–289.

Iman, A., Johnson, G.C., 1998. Decomposition of the deformation gradient in thermoelasticity. ASME J. Appl. Mech. 65, 362–366.

Lubliner, J., 1984. A maximum-dissipation principle in generalized plasticity. Acta Mech. 52, 225–237.

Lubliner, J., 1987. Non-isothermal generalized plasticity. In: Bui, H.D., Nguyen, Q.S. (Eds.), Thermomechanical Coupling in Solids. IUTAM, North-Holland.

Lee, E.H., 1969. Elasto-plastic deformation at finite strain. ASME J. Appl. Mech. 36, 1–6.

Mandel, J., 1973. Equations constitutives et directeurs dans les milieux plastiques et viscoplastiques. Int. J. Solids Struct. 9, 725–740.

Marsden, J.E., Hughes, T.J.R., 1983. Mathematical Foundations of Elasticity. Prentice Hall, Englewood Cliffs, NJ.

Miehe, C., Stein, E., 1992. A canonical model of multiplicative elasto-plasticity. Formulation and aspects of numerical implementation. Euro. J. Mech. A/Solids 11, 25–43.

Needleman, A., 1988. Material rate dependence and mesh sensitivity in localization problems. Comput. Methods Appl. Mech. Engng. 67, 69–85.

Perić, D., Owen, D.R.J., Honnor, M.E., 1992. A model for finite strain elasto-plasticity based on logarithmic strains: computational issues. Comput. Methods Appl. Mech. Engng. 94, 35–61.

Simo, J.C., 1992. Algorithms for static and dynamic multiplicative plasticity that preserve the classical return mapping schemes of the infinitesimal theory. Comput. Methods Appl. Mech. Engng. 99, 61–112.

Simo, J.C., Miehe, C., 1992. Associated coupled thermoplasticity at finite strains: formulation, numerical analysis and implementation. Comput. Methods Appl. Mech. Engng. 98, 41–104.

Strang, G., 1986. Introduction to Applied Mathematics. Wellesley-Cambridge Publ. Co, Wellesley, MA.

Truesdell, C., Noll, W., 1965. In: The Nonlinear Field Theories of Mechanics in Handbuch der Physik, vol. III. Springer, Berlin.

Weber, G., Anand, L., 1990. Finite deformation constitutive equations and a time integration procedure for isotropic, hyperelastic-viscoplastic solids. Comput. Methods Appl. Mech. Engng. 79, 173–202.

Wriggers, P., Miehe, C., Kleiber, M., Simo, J.C., 1992. On the coupled thermomechanical treatment of necking problems via finite element methods. Int. J. Numer. Methods Engng. 33, 869–883.

Zienkiewicz, O.C., Taylor, R.L., 1989. The Finite Element Method: Basic Formulation and Linear Problems. McGraw-Hill, London.